Journal of Nanobiotechnology

RESEARCH

Open Access

Dendritic mesoporous silica-delivered siRNAs nano insecticides to prevent *Sogatella furcifera* by inhibiting metabolic detoxification and reproduction

Changwei Gong[1,2], Wei Wang[3*], Yanxin Ma[2], Xiaoxu Zhan[4], Anchun Peng[2], Jian Pu[2], Jizhi Yang[2] and Xuegui Wang[1,2*]

Abstract

Background Migratory insect infestation caused by *Sogatella furcifera* is a serious threat to rice production. The most effective method available for *S. furcifera* control is intensive insecticide spraying, which cause widespread resistance. RNA interference (RNAi) insecticides hold enormous potential in managing pest resistance. However, the instability and the poor efficiency of cross-kingdom RNA trafficking are key obstacles for the application in agricultural pest management.

Methods We present dendritic mesoporous silica nanoparticles (DMSNs)-based nanocarrier for delivering siRNA and nitenpyram to inhibit the metabolic detoxification and development of *S. furcifera*, thereby preventing its proliferation.

Results This nano complex (denoted as N@UK-siRNA/DMSNs) significantly enhanced the stability of siRNA (efficacy lasting 21 days) and released cargos in GSH or planthopper bodily fluid with a maximum release rate of 84.99%. Moreover, the released UK-siRNA targeting two transcription factors (*Ultraspiracle* and *Krüppel-homolog 1*) downregulated the developmental genes *Ultraspiracle* (0.09-fold) and *Krüppel-homolog 1* (0.284-fold), and downstream detoxification genes ABC *SfABCH4* (0.016-fold) and P450 *CYP6FJ3* (0.367-fold).

Conclusion The N@UK-siRNA/DMSNs inhibited pest development and detoxification, significantly enhancing susceptibility to nitenpyram to nanogram level (LC_{50} is 250–252 ng/mL), resulting in a 5.37–7.13-fold synergistic ratio. This work proposes a comprehensive management strategy for controlling *S. furcifera* to ensure the green and safe production of rice.

Keywords *Sogatella furcifera*, Insecticide resistance management, RNAi pesticides, Insecticides delivery, Dendritic mesoporous silica nanoparticles

*Correspondence:
Wei Wang
wwei@sicau.edu.cn
Xuegui Wang
wangxuegui@sicau.edu.cn
Full list of author information is available at the end of the article

Graphical Abstract

Schematic fabrication of the N@UK-siRNA/DMSNs and the molecular mechanism resolution of improving the sensitivity of *S. furcifera* to nitenpyram. The nitenpyram and UK-siRNA are assembled onto the DMSNs by interfacial modification. With phloem and xylem pathway, the N@UK-siRNA/DMSNs could transport bi-directionally to the feeding sites of *S. furcifera* and then release nitenpyram and UK-siRNA in *S. furcifera* in response to glutathione (GSH). The UK-siRNA released from N@UK-siRNA/DMSNs would downregulate the developmental genes *USP* and *Kr-H1*. The releasing nitenpyram would competitively bind to acetylcholine (ACh) receptors, inhibiting the transmission of nerve impulses

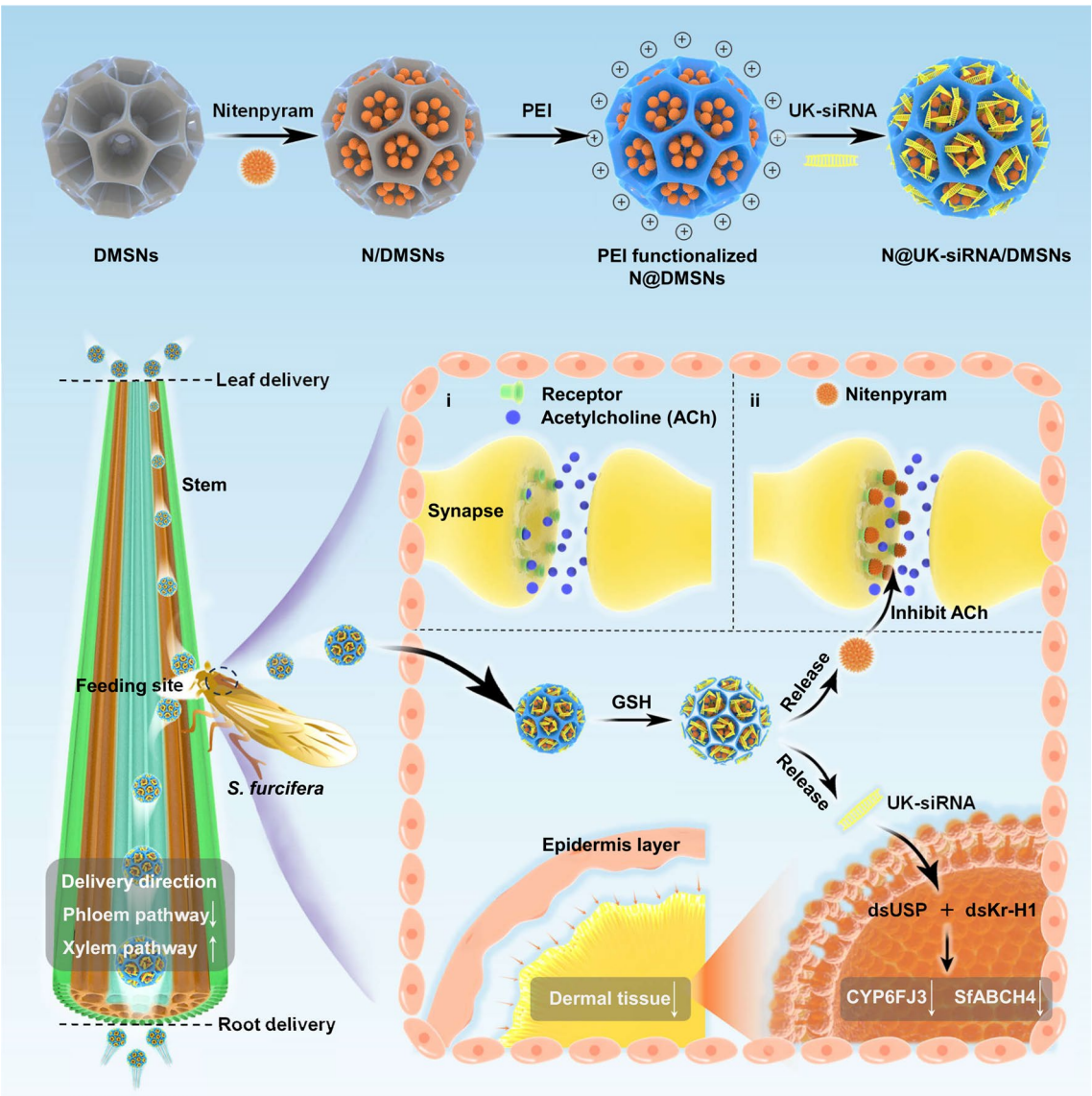

Introduction

Migratory insect infestation caused by *Sogatella furcifera* (*S. furcifera*) is a serious threat to food security in rice-producing regions of China and other parts of Asia. It belongs to the Delphacidae family in the Homoptera order, and is notorious for its long-distance migration, rapid reproduction, and large-scale outbreaks [1]. By directly feeding on the phloem sap of rice in the adult

and nymph stages, *S. furcifera* causes stunted growth, delayed tillering, increased percentage of empty grains, and even death of the entire plant, which is known as "hopperbrun" [2]. Additionally, *S. furcifera* is a vector for various pathogens, such as *Rice Black Streaked Dwarf* Virus and *Rice Stripe* Virus. Hence, *S. furcifera* is a key pest targeted for control and management by the Ministry of Agriculture and Rural Affairs of the People's Republic of China [3]. Currently, the almost exclusive method for controlling *S. furcifera* relies on the chemical insecticides, such as organophosphates, neonicotinoids and insect growth regulators [4]. Nonetheless, prolonged and indiscriminate use of chemical insecticide has led to significant resistance in the *S. furcifera* against multiple classes of insecticides including chlorpyrifos, nitenpyram, and pymetrozine [5–8]. The widespread dissemination of resistance and resurgence of the pest have further exacerbated the irrational use of chemical insecticides and environmental pollution, creating a vicious cycle of worsening infestations [9]. Therefore, environmentally friendly approaches should be explored for reducing dosage, decreasing pollution and resistance management.

RNA interference (RNAi) insecticides have shown tremendous potential in pest resistance management and integrated pest management, compared with the chemical insecticide targeting insect neurology, endocrinology and digestive system which shows extended development cycles and high costs [10–12]. RNAi insecticides could specifically inhibit the expression of resistance or development-related mRNA triggered by endogenous or exogenous RNA and not cause damage to non-target species, resulting in adaptation to environment, sensitivity to chemical insecticides or mortality in target pests [13]. With the increasing popularity of ecological concepts such as avoiding biological contamination and sustainable development, some types of RNA-based bioinsecticides have been approved by United States Environmental Protection Agency [14, 15]. However, the low efficiency of small interfering RNA (siRNA) delivery to target pests, the instability of siRNA, and the low residual concentration in insect bodies are key obstacles for the commercialization of RNAi insecticides in agricultural pest management [16]. With the assistance of nanoparticles, direct spraying of siRNA-loaded nanoparticles that exhibit stability and could target key genes of pest onto crops (Spray-Induced Gene Silencing, SIGS) is hopeful to induce specific silencing, disrupt the growth and reproduction of pest, thus controlling or preventing crop pest [17–19]. For example, *S. furcifera* mainly feeds on rice phloem sap using its stylet. If the siRNA-loaded nanoparticles could enrich in rice stem, cross species barriers, enter the pest's body, the key obstacles of RNAi pesticides on *S. furcifera* would be overcome [20, 21]. Therefore, the SIGS strategy requires a reliable nanocarrier for plant transport.

Herein, we introduce dendritic mesoporous silica nanoparticles (DMSNs) as a nanocarrier for siRNA to prevent the proliferation of *S. furcifera* by inhibiting its metabolic detoxification and development (Graphical abstract). The DMSNs with a diameter around 100 nm which exhibit high specific surface area, biocompatibility and efficiency of cellular internalization can overcome the bottleneck of siRNA delivery to target pests and extend the protective window of RNA interference, enhance siRNA stability, and improve its intracellular delivery efficiency [22–25]. Moreover, the siRNA (denoted as UK-siRNA) targeting two transcription factors (*Ultraspiracle* and *Krüppel-homolog 1*, denoted as *USP* and *Kr-h1*, actively) and nitenpyram were assembled on the DMSNs. This nano complex (denoted as N@UK-siRNA/DMSNs) significantly enhanced the stability of UK-siRNA. Through both symplastic and apoplastic pathways, it transported bi-directionally to the feeding sites of planthoppers via the phloem and xylem tissues, where induced the N@UK-siRNA/DMSNs releasing nitenpyram and UK-siRNA by GSH or planthopper bodilyfluid and exhibited negligible toxicity to rice. With the delivery of UK-siRNA, the N@UK-siRNA/DMSNs significantly downregulated the developmental genes *USP* and *Kr-H1*, and downstream detoxification genes ABC *SfABCH4* and P450 *CYP6FJ3*. Consequently, the N@UK-siRNA/DMSNs inhibited pest growth and development, significantly enhancing susceptibility to nitenpyram to nanogram level (LC_{50} reduced from 1.353–1.782 μg/mL to 250–252 ng/mL), resulting in a 5.37–7.13-fold synergistic ratio. And thus, the multicomponent nano delivery system provides a comprehensive management strategy for controlling *S. furcifera* to ensure the green and safe production of rice and other staple crops.

Materials and methods

Test insects

The HN-Lab strain of *S. furcifera* was initially introduced from Professor Youzhi Li's research group at College of Plant Protection, Hunan Agricultural University in 2015. This strain has been diligently maintained for 15 years, devoid of any exposure to insecticides. In contrast, the JL21 strain, renowned for its robust resistance to pymetrozine, was gathered from a population in Junlian, Sichuan in 2021. This strain underwent rigorous screening for 6 consecutive generations, using a LC_{50} dosage of pymetrozine. The entire generation of *S. furcifera* was reared in insect cages on conventional rice seedlings (cultivar TN1), while the rice seedlings were

grown hydroponically. The laboratory rearing conditions include a temperature of 26 ± 1 °C, relative humidity of 85% ± 5%, and a photoperiod of 14L:10D.

Synthesis of nano-material N@UK-siRNA/DMSNs

A 0.34 g triethanolamine was dissolved in 125 mL water and stirred vigorously at 80 °C for 0.5 h. Subsequently, 1.9 g cetyltrimethylammonium bromide and 0.84 g sodium salicylate were added, and the mixture was further stirred for 1 h. Following this, 8 mL bis-(γ-triethoxysilylpropyl)-tetrasulfide and 10 mL tetraethyl orthosilicate were introduced, and the solution was stirred for 12 h. The resulting particles were then centrifuged and thoroughly washed with ethanol. To effectively remove the surfactant, a mixture of 0.5 mL of 38% HCl and 30 mL of 99.7% ethanol was added, and the suspension was heated at 60 °C for 6 h. This process was repeated three times. The DMSNs were then vacuum-dried at room temperature, following a previously reported protocol [23]. For loading, 30 mg nitenpyram and 60 mg DMSNs were dispersed in 60 mL methanol and stirred at room temperature for 4 h. The mixture was centrifuged at 12,000 rpm for 20 min, and the precipitate was collected and washed with methanol three times. Subsequently, 60 mg of DMSNs-Nitenpyram were dispersed in 15 ml of a 1 mg/mL polyethyleneimine (PEI) solution, stirred at 250 rpm for 4 h at room temperature. Excess PEI was removed via centrifugation at 12,000 rpm for 20 min, and the precipitate was washed with deionized water.

UK-siRNA, simultaneously targeting *USP* and *Kr-H1*, was designed using siDirect (http://sidirect2.rnai.jp/) based on the gene sequences of *USP* and *Kr-H1* in *S. furcifera*. The UK-siRNA was synthesized and constructed into the L4440 vector. L4440-UK-siRNA was transformed into HT115 (DE3), and dsUK-siRNA (double-stranded siRNA targeting USP and Kr-H1) was expressed according to the method described by Gong et al. [24]. Finally, 30 mg RNA and 60 mg DMSNs-Nitenpyram-PEI were added to 60 mL ethanol and stirred for 24 h at room temperature. After centrifugation again to remove any free RNA, the N@UK-siRNA/DMSNs nanoparticles were obtained.

Characterization of N@UK-siRNA/DMSNs

The freeze-dried N@UK-siRNA/DMSNs nanoparticles were thoroughly characterized using various techniques. For scanning electron microscopy (SEM) analysis, 3 mg of the nanoparticles were dispersed in 10 mL of distilled water and sonicated for 5 min. The suspension was then applied to conductive adhesive-coated metal discs, followed by gold sputter coating for 45 s under vacuum conditions. The coated samples were observed under a Zeiss GeminiSEM 360 SEM at an accelerating voltage of 15 kV to assess their morphological structure. To further investigate the morphology, distribution, and particle size of the nanoparticles, transmission electron microscopy (TEM) was performed using a Japan Jeol 2100 Plus TEM. A few drops of the nanoparticle suspension were deposited onto copper grids and allowed to air-dry overnight on filter paper before analysis. Additionally, Energy Dispersive X-ray Spectroscopy (EDS) mapping was performed for compositional analysis. Particle size distribution and Zeta Potential were measured using a Malvern Zetasizer Nano S90 liquid Zeta sizer. Prior to analysis, the nanoparticles were dispersed in deionized water and sonicated for 10 min. Fourier transform infrared (FTIR) spectroscopy was employed to obtain spectral information about the nanoparticles. Specifically, 1 mg of the sample was ground with approximately 150 mg of dry KBr in an agate mortar and pressed into pellets. The pellets were analyzed in the range of 400–4000 cm^{-1} using standard KBr pellet technique. Finally, X-ray photoelectron spectroscopy (XPS) was utilized for elemental composition analysis of the nanoparticles. Both survey and high-resolution scans were performed using a Thermo Scientific NEXSA XPS system. The results from these comprehensive characterization techniques provide valuable insights into the properties and composition of the N@UK-siRNA/DMSNs nanoparticles.

Release study of N@UK-siRNA/DMSNs

0.05 g of N@UK-siRNA/DMSNs nanoparticles were individually dissolved in 25 mL of phosphate-buffered saline (PBS, pH 7.4), PBS2 (containing 1 mM GSH), PBS3 (containing 10 mM GSH), and a bodily fluid diluent (consisting of 10 mg bodily fluid diluted in l mL PBS). For each solution, 5 mL was placed into a dialysis bag and subsequently immersed in 30 mL of pH 7.4 PBS, ensuring complete submersion. At predetermined time intervals, 1 mL of the external buffer solution was removed and replenished with an equal volume of fresh buffer solution. The withdrawn solutions were analyzed for absorbance using UV–Vis spectroscopy, and the nitenpyram content at each time point was determined using a standard curve for the pyridine insecticide.

Biological evaluation of N@UK-siRNA/DMSNs

The toxicity of *S. furcifera* to the nanoparticles and nitenpyram was assessed employing both seed soaking and root soaking techniques. Nitenpyram was initially dissolved in dimethyl sulfoxide and then diluted with a 0.1% Triton solution to achieve varying concentrations. In parallel, nanoparticles with equivalent nitenpyram concentrations were also prepared using a 0.1% Triton solution. Rice seedlings were treated with these prepared solutions

using either seed soaking or root soaking methods. After treatment, third-instar nymphs of *S. furcifera* were introduced to the seedlings. Each concentration was tested on 15 nymphs, with the experiment repeated at least three times. Untreated groups served as blank controls for comparison. After 3 days, nymphs that exhibited immobility or death were considered deceased. The deceased nymphs, which had been exposed to different concentrations of nanoparticles and nitenpyram, were fixed in 4% paraformaldehyde. They were then dehydrated using a graded ethanol–water series and subjected to histological hematoxylin and eosin (HE) staining following standard procedures. This included paraffin embedding, sectioning, deparaffinization, staining, dehydration, and mounting of the tissue sections.

Real-time fluorescent quantitative PCR

Approximately 50 mg third-instar nymphs of *S. furcifera* were homogenized, and mRNA from different treatment groups was extracted using the RNA-easy Isolation Reagent kit from Nanjing Nuoweizan Biotechnology Co., Ltd., following the provided instructions. Reverse transcription experiments were conducted according to the instructions of the NovoScript Plus 1st Strand cDNA Synthesis kit from Suzhou Novoprotein Technology Co. Ltd. Initially, 1 μg mRNA was mixed with 1 μL gDNA Purge and an appropriate amount of RNase-free H_2O, incubated at 42 °C for 5 min to remove gDNA, followed by the addition of 10 μL 2 × SuperMix, incubated at 40 °C for 10 min and then at 75 °C for 5 min to prepare cDNA. To determine the relative expression of different genes (Table S1) in *S. furcifera*, Real-Time PCR was performed using the RPL9 gene as the reference gene. The reaction system comprised 10 μL SYBR Premix Ex Taq TM, 1 μL each of forward and reverse primers (5 μmol/L), 7 μL ddH_2O, and 1 μL cDNA template, making up a total volume of 20 μL. The reaction conditions were as follows: 95 °C for 1 min, followed by 40 cycles of 95 °C for 20 s, 60 °C for 20 s, and 72 °C for 30 s. Finally, a melting curve was generated by gradually increasing the temperature from 60 °C to 95 °C at a rate of 0.2 °C/s. Each gene was measured in triplicate, and the relative gene expression levels were calculated using the $2^{-\triangle\triangle Ct}$ method. Changes in the expression levels of *USP* and *Kr-H1*, as well as detoxification metabolic genes (*CYP6FJ3*, *CYP6CS3*, etc.), were determined at 24 and 48 h after treatment with sublethal doses of N@UK-siRNA/DMSNs in third-instar nymphs.

Fluorescence in situ hybridization

Immediately after being washed, the tissues were promptly fixed in a fixative solution (prepared with DEPC water) for a duration ranging from 2 to 12 h. Following fixation, the tissues underwent a series of dehydration steps in an alcohol gradient, infiltration with wax, and eventual embedding. The paraffin-embedded tissues were then precisely sectioned using a microtome, mounted onto slides with the aid of a slide warmer, and incubated in a 62 °C oven for 2 h to ensure proper adherence. The sections were subsequently processed in a series of solvents, beginning with xylene I for 15 min, followed by xylene II for another 15 min. This was then followed by a gradient of alcohol washes, including absolute ethanol I and II for 5 min each, 85% ethanol for 5 min, and 75% ethanol for 5 min. The sections were then rinsed with DEPC water. Depending on the duration of tissue fixation, the sections were subjected to boiling in a repair solution for 10–15 min, allowing them to cool naturally afterwards. After outlining the target genes, proteinase K (20 μg/mL) was carefully applied dropwise, and the sections were incubated at 37 °C for 20–30 min to facilitate digestion. This was followed by rinsing with distilled water and three washes with PBS, each lasting 5 min. The pre-hybridization solution was then applied, and the sections were incubated at 37 °C for 1 h. After removing the pre-hybridization solution, hybridization was carried out overnight at 37 °C using a hybridization solution containing specific probes (USP: 5'-FAM CCGCCTCCA GAATCCTTTCGATTGGCATGTCTGTGTGGAAAC TGCTGGTTGATTCGACC; Kr-H1: 5'-CY3 AGAGCG GAGCAGCTGGCTCAGAGTGACTCTTGATGTGGC CTTCCATTGTTTTC TTTGAG; SfABCH4: 5'-FITC TCAATAATTGCGGATCATGAAGTAGAGCTACAC). Post-hybridization, the sections were washed thoroughly with 2 × SSC at 37 °C for 10 min, followed by 1 × SSC at 37 °C for 5 min (repeated once) and 0.5 × SSC at room temperature for 10 min. If any nonspecific hybridization was observed, additional formamide washing was performed as necessary. The sections were then stained with 4',6-diamidino-2-phenylindole (DAPI) staining solution, incubated in the dark for 8 min, rinsed, and mounted using an anti-fade mounting medium. The processed sections were carefully observed and images were captured under a Nikon upright fluorescent microscope, utilizing the appropriate excitation and emission wavelengths for FAM (488 nm excitation, 465–495 nm emission, and 515–555 nm detection).

RNAi of metabolic resistance-related transcription factors

Firstly, *SfABCH4, USP* and *Kr-H1* sequences containing the T7 promoter (Table S2) were amplified according to Zhang et al. [25] and purified using the FastPure® Gel DNA Extraction Mini Kit (Nanjing Vazyme Biotech Co., Ltd.). dsSfABCH4, dsUSP, dsKr-H1, and dsGFP were synthesized and purified using the T7 RNAi Transcription Kit-BOX1 (Nanjing Vazyme Biotech Co., Ltd.) following

the manufacturer's instructions, and their concentrations and qualities were determined using a microspectrophotometer. Fourth-instar larvae of the JL21 strain were anesthetized for 30 s and then placed on plates containing 1% agar, with wells made using toothpicks. Using the UMP3/Nanoliter2010 microinjection system (World Precision Instruments), each larva was injected with 40 nL of solution containing 150 ng of dsRNA. After injection, qRT-PCR was performed at 24 and 48 h to assess the expression of *USP*, *Kr-H1*, and ABC genes. At 48 h post-injection, larvae treated with dsUSP, dsKr-H1, and dsGFP were separately fed with 0.25 μg/mL and 0.5 μg/mL of nitenpyram, and the mortality rates were recorded three days after treatment.

Determination of dispersion of composite nano-insecticides

Fluorescein isothiocyanate (FITC)-labeled composite nano-materials were employed to investigate the absorption and distribution patterns on rice leaves. The leaves were submerged in a solution containing FITC-labeled nano-carriers. To assess the translocation of nano-carriers from the roots to other sections of the plant, rice seedlings were grown in a solution enriched with nanomaterials. Subsequently, the treated rice seedlings were exposed to S. furcifera and incubated under controlled conditions of 25 °C temperature, a 16:8 (L:D) photoperiod, and 75% humidity. After 24 h, the distribution of FITC-labeled nano-carriers within various parts of the rice plant and inside *S. furcifera* was visualized using laser confocal microscopy, utilizing an excitation wavelength of 488 nm.

Yeast one-hybrid assay

A single yeast colony was selected and propagated overnight in YPDA liquid medium. The culture was centrifuged at 1000×*g* for 5 min, and the supernatant was discarded. The yeast pellet was resuspended in a one-step buffer containing 100 μL of 2 M LiAc (pH 7.5), 800 μL of 50% PEG4000, and 100 μL of 1 M DTT to prepare competent yeast cells. Prior to use, carrier DNA underwent heat treatment at 95 °C for 5 min, followed by an ice bath, and then repeated with another cycle of 95 °C for 5 min and an ice bath. A plasmid mixture containing 2–3 μg of the plasmid to be transformed was combined with 5 μL of the pretreated carrier DNA and added to the competent yeast cells. The mixture was incubated at 42 °C for 1 h. The transformed yeast was then plated onto an SD-Leu-Trp medium plate, dried, sealed, and incubated at 28 °C for 2 days until colonies appeared. The colonies were diluted 100 times using sterile water, mixed thoroughly, and 100 μL was plated onto SD-Leu-Trp-His medium supplemented with 50 mM 3-amino-1,2,4-triazole (3AT). The plates were dried, sealed, and incubated at 28 °C for 2 days before observation.

Results and discussion

Construction and in vitro insecticidal characterization of N@UK-siRNA/DMSNs.

We sequentially utilized triethanolamine, cetyltrimethylammonium bromide, and sodium salicylate, followed by the addition of bis-[γ-(triethoxysilyl)propyl] tetrasulfide and tetraethyl orthosilicate, to prepare negatively charged DMSNs. After loading nitenpyram, the nanoparticles were coated with PEI to render them positively charged for loading UK-siRNA, ultimately obtaining N@UK-siRNA/DMSNs (Fig. 1a). Under SEM observation, N@UK-siRNA/DMSNs exhibited uniformly spherical structures with a diameter of approximately 100 nm and surface wrinkles, these wrinkles were attributed to the attachment of many porous channels and tubular structures in the material (Fig. 1b, S1). This structural feature notably contrasted with the findings reported by Wang et al., where wrinkles were densely distributed without the presence of attached tubular structures [26]. In TEM images, the spherical nanoparticles also demonstrated uniformity in size, featuring internal branching structures characterized by darker central regions and lighter peripheral fillings, and its diameter was about 140 nm with many channels of 20–60 nm length (Fig. 1c–e, S2). Upon magnification, these branch-like structures were observed extending and growing randomly from the central regions towards the periphery, resembling the structural characteristics of dendritic mesoporous silica nanoparticles [27]. Elemental mapping using TEM energy-dispersive spectroscopy revealed similar shapes and distributions of elements such as nitrogen (N), carbon (C), oxygen (O), chlorine (Cl), phosphorus (P) and silicon (Si) within the nanoparticles, confirming the composition of the nanomaterial (Fig. 1f). Specifically, the mass percentages of these elements were 5.49% for N, 42.64% for C, 28.42% for O, and 22.65% for Si, respectively (Fig. 1f). Notably, the elemental shape of P, a characteristic element of RNA, closely resembled the shape of the nanomaterial, with a moderate density observed within some spherical structures, accounting for 0.78% of the total mass (Fig. 1f). Similarly, the elemental shape of Cl, a characteristic of nitenpyram, aligned with the nanomaterial structure and comprised 0.01% of the mass (Fig. 1f). Dynamic light scattering measurements revealed that the particle size distribution of N@UK-siRNA/DMSNs ranged from 79 to 220 nm (Polydispersity Index, PDI, 0.173 ± 0.014), with the majority (73.51% of the total) concentrated between 106 and 142 nm (Fig. 1g,

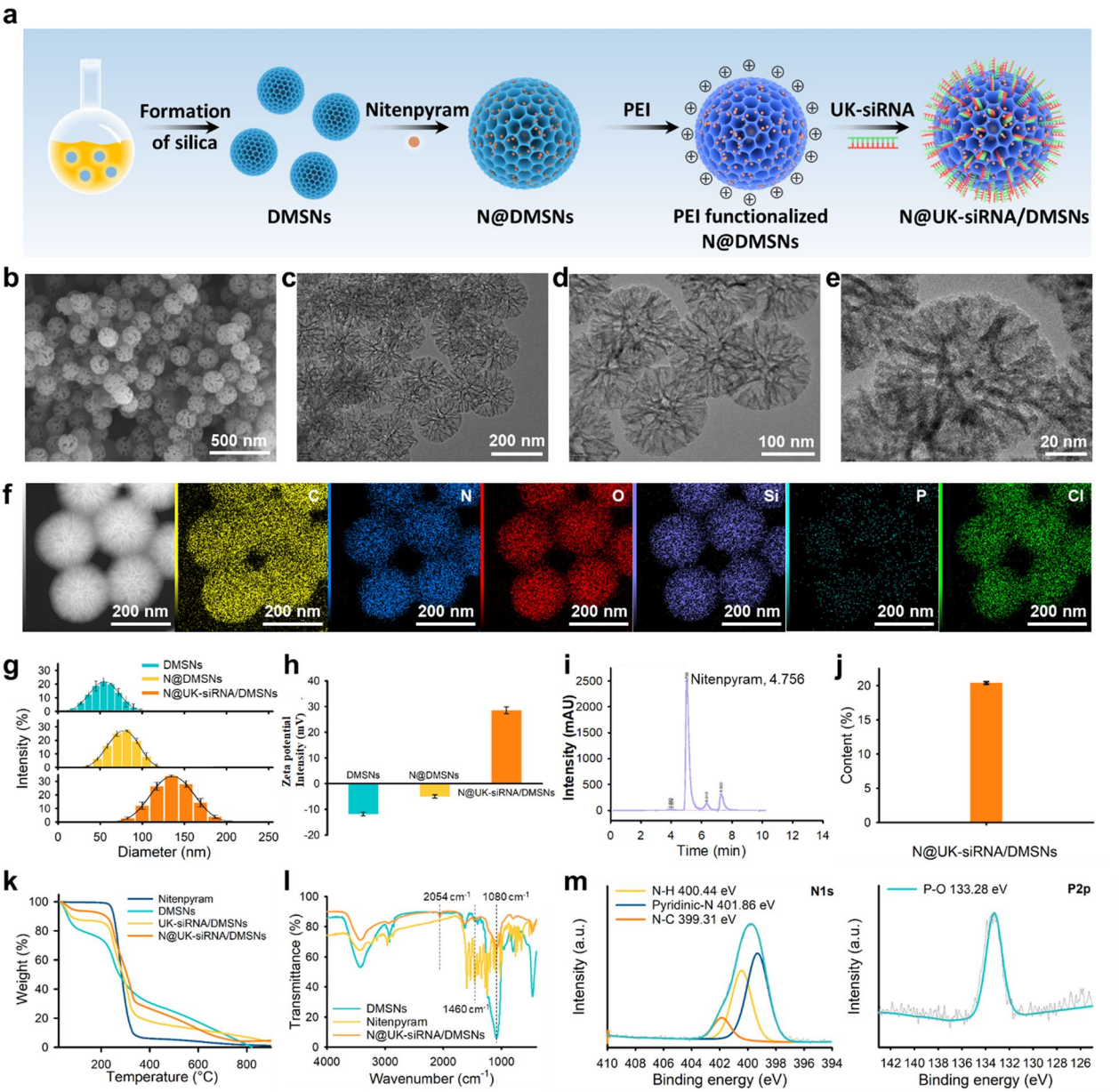

Fig. 1 Preparation and characterization of N@UK-siRNA/DMSNs. **a** The schematic diagram of the preparation process of N@UK-siRNA/DMSNs. **b–e** High-magnification morphology features under SEM (**b**) at 10,000 scales and TEM (**c–e**) at 15,000, 50,000 and 150,000 scales, respectively. **f** Elemental mapping of C, N, O, Si, P, and Cl elemental spectra using TEM energy-dispersive spectroscopy. Distribution of particle size (**g**) and Zeta Potential (**h**) of N@DMSNs, DMSNs, and N@UK-siRNA/DMSNs. **i**, **j** The content of nitenpyram in N@UK-siRNA/DMSNs nanoparticle determined by high performance liquid chromatography. **k** The thermogravimetry of DMSNs, UK-siRNA/DMSNs, nitenpyram and N@UK-siRNA/DMSNs. **l** The FTIR spectra of DMSNs, nitenpyram and N@UK-siRNA/DMSNs. **m** The XPS fine spectrum analysis of N@UK-siRNA/DMSNs, such as N1s and P2p, other XPS results please see SUPPORTING INFORMATION

S5), following a bimodal discrete probability distribution similar to that reported by Kienzle et al. [28]. This distribution was notably wider than those observed for N@DMSNs (44–122 nm, PDI, 0.086 ± 0.027) and DMSNs (28–122 nm, PDI, 0.081 ± 0.014), indicating a greater degree of size variation among the N@UK-siRNA/DMSNs (Fig. 1g, S5). The particle size data indicated that after assembling nitenpyram and RNA, the diameter of the nanoparticles increased. The measured Zeta Potential of N@UK-siRNA/DMSNs was 28.6 mV, which was higher than those observed for N@DMSNs (− 5.0 mV) and DMSNs (− 11.8 mV) (Fig. 1h). The Zeta Potential

distribution of the nanoparticles showed obvious characteristic peaks, with peak values at 30.1 mV (Fig. S3), indicating negatively charged surfaces of the DMSN particles [29], ensuring their stability in the suspension. The addition of the cationic polymer PEI results in an increase in the positive charge of N@UK-siRNA/DMSNs, facilitating the loading of more RNA molecules [30]. Consequently, the prepared dendritic mesoporous silica DMSNs demonstrated the capability to load siRNA and nitenpyram effectively.

It was found by high performance liquid chromatography that a distinct peak was observed in the retention time of 4.756 min for the N@UK-siRNA/DMSNs solution, with a peak area of 4116.6 (Fig. 1i). Utilizing the standard curve of nitenpyram (concentration of nitenpyram $y = 0.0167x - 3.7352$, $R^2 = 0.999$), the loading rate of nitenpyram in N@UK-siRNA/DMSNs was calculated to be 20.4% (Fig. 1j). Examining the thermal stability through residual mass percentages, it was observed that between 25 °C and 271 °C, nitenpyram retained a higher mass percentage (67.3%–100.0%) compared to N@UK-siRNA/DMSNs (59.1%–100.0%), UK-siRNA/DMSNs (67.1%–100.0%), and DMSNs (50.8%–100.0%). Within the temperature range of 271 °C to 280 °C, the residual mass of nitenpyram (54.5%–67.3%) and UK-siRNA/DMSNs (62.8%–67.1%) remained higher than that of N@UK-siRNA/DMSNs (53.9%–59.1%) and DMSNs (48.2%–50.8%) (Fig. 1k). From 280 °C to 285 °C, the residual mass of nitenpyram (48.2%–54.5%), UK-siRNA/DMSNs (59.9%–62.8%), and N@UK-siRNA/DMSNs (51.6%–59.1%) surpassed that of DMSNs (47.1%–50.8%) (Fig. 1k). However, within the broader temperature range of 271 °C to 801 °C, nitenpyram showed a lower residual mass percentage (1.6%–54.5%) compared to N@UK-siRNA/DMSNs (6.8%–51.6%), UK-siRNA/DMSNs (4.1%–59.9%), and DMSNs (1.7%–47.1%) (Fig. 1k). Compared to the FTIR spectra of DMSNs and nitenpyram, N@UK-siRNA/DMSNs exhibited a distinct absorption peak at 2054 cm^{-1} (Fig. 1l), according to the CO residue in the base of RNA [31]. Both nitenpyram and N@UK-siRNA/DMSNs showed a prominent absorption peak at 1460 cm^{-1} (Fig. 1l), associated with the deformation vibration of C-H in the pyridine ring of nitenpyram. Following the introduction of PEI onto DMSNs (Fig. 1l), characteristic stretching vibration peaks emerged, such as NH at 1590 cm^{-1} [32]. Both N@UK-siRNA/DMSNs and DMSNs exhibited an absorption peak at 1080 cm^{-1}, which is attributed to the stretching vibration of Si–O-Si bonds, a signature peak of silica materials (Fig. 1l). XPS analysis of N@UK-siRNA/DMSNs revealed the presence of elements including N, C, O, P, Cl, and Si (Fig. 1m, S4). The C1s XPS spectrum exhibited three peaks at 284.80, 288.34, and 286.32 eV (Fig. 1m, S4), corresponding to C–C, C–O, and C–N chemical bonds, respectively [33]. The N1s XPS spectrum displayed three peaks at 400.44, 401.34, and 399.31 eV (Fig. 1m), attributed to N–H, N-Pyridine, and N–C chemical bonds, respectively. The O1s XPS spectrum showed two peaks at 531.32 and 532.70 eV (Fig. S4), associated with O–Si and O=C/N chemical bonds [34]. The P2p XPS spectrum exhibited a single peak at 133.28 eV (Fig. 1m), indicating P–O chemical bonds [35], while the Si2p XPS spectrum displayed a peak at 102.97 eV (Fig. S4), corresponding to Si–O chemical bonds [36]. Therefore, N@UK-siRNA/DMSNs successfully loaded a higher amount of nitenpyram and carried RNA.

To test the corresponding release performance of N@UK-siRNA/DMSNs, the N@UK-siRNA/DMSNs were individually immersed in PBS (pH 7.0) containing 0, 1, and 10 mM GSH, as well as in bodily fluid (10 mg/mL, PBS) for 24 h, 84 h and 160 h to observe the particle states using SEM. In the PBS solution without GSH (0 mM), we observed a consistently high particle density, accompanied by strong cohesion between particles and robust particle integrity (Fig. 2a). In the presence of 1 mM GSH, the particle density gradually decreased over time, exhibiting weaker cohesion yet maintaining strong particle integrity (Fig. 2b). However, in the 10 mM GSH solution, the particle density declined rapidly, with the remaining particles aggregating into clusters and most particles fragmenting (Fig. 2c). Similarly, in the bodily fluid diluent, the particle density also rapidly decreased, resulting in clusters of particles and a significant number of fragmented particles (Fig. 2d). Real-time monitoring of the nitenpyram content in the solutions revealed that at 1, 14, 38, 62, 84, 108, 132, 160, 184, and 208 h, the release rate of nitenpyram was highest in the bodily fluid diluent (ranging from 17.7% to 84.99%), followed by the 10 mM GSH solution (18.2% to 77.0%) and the 1 mM GSH (9.2% to 27.3%), and the 0 mM GSH solutions (2.6% to 15.5%) was lowest (Fig. 2e, f). When PEI-modified DMSNs were added to a 1 mg/mL RNA solution in ratios of 1:10, 1:5, 3:10, and 1:2, the brightness of the nucleic acids in the dot holes increased proportionately with the ratio (Fig. 2g). Notably, the brightness of the nucleic acids in the dot holes remained relatively stable after 3, 6, 9, 12, 15, 18, and 21 days when N@UK-siRNA/DMSNs were placed in a 0.5 mg/mL RNA solution (Fig. 2h). Wang et al. [26] found that DMSNs-CHL-PEI-SPI significantly increased the release of chemical insecticides in alkaline solutions containing GSH, similar to the results of this experiment. Moreover, *S. furcifera* nymphs were rich in the reducing substances containing GSH, which could also accelerate the release of nitenpyram [37]. Meanwhile, the addition of GSH could induce the collapse of the disulfide bond (–S–S–) structure within the framework of DMSNs,

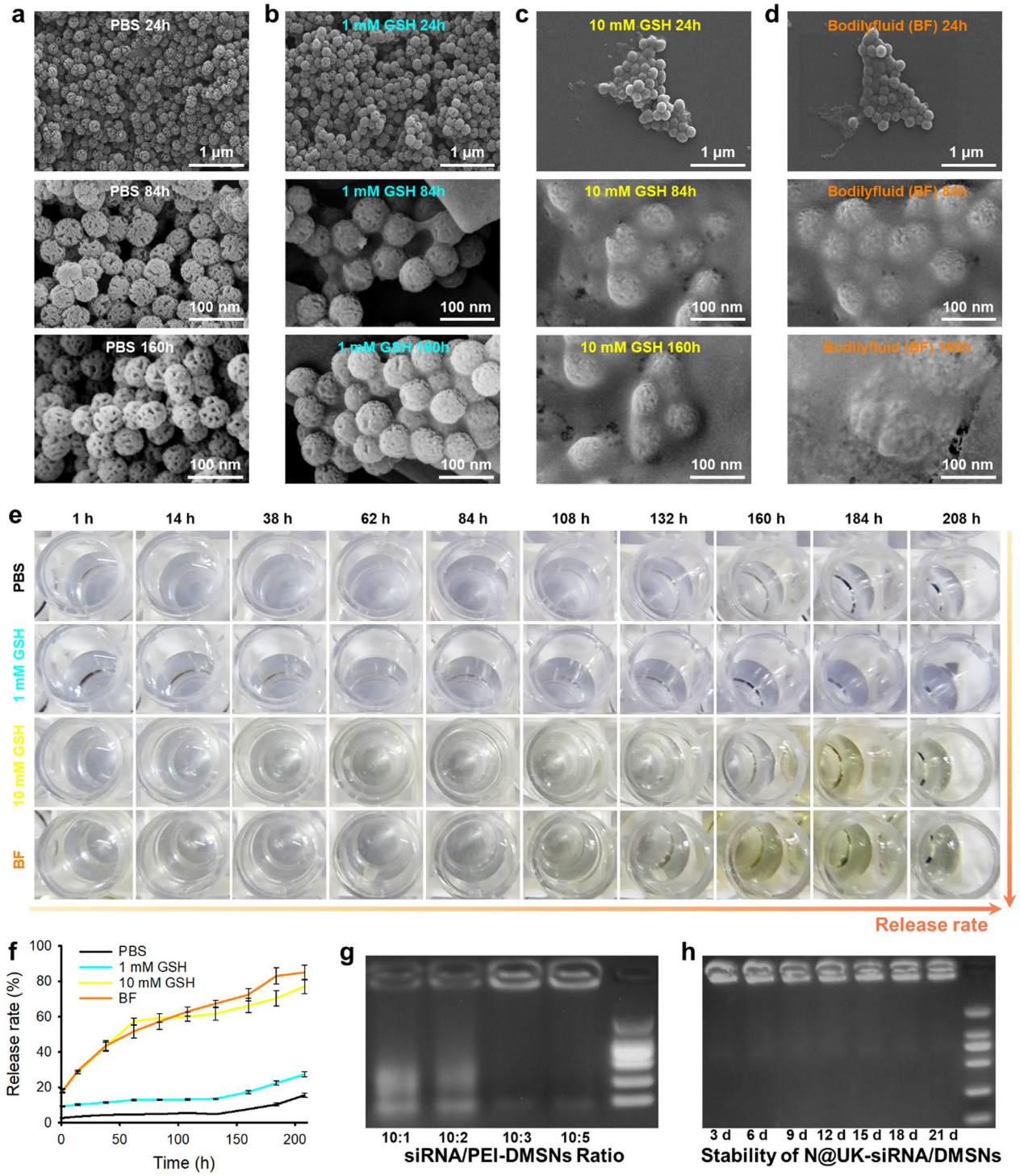

Fig. 2 Controllable release of N@UK-siRNA/DMSNs. **a**–**d** The morphology of N@UK-siRNA/DMSNs after 24, 84 and 160 h placed in in PBS (pH 7.0) containing 0 (**a**), 1 (**b**), and 10 mM (**c**) mM GSH, and bodilyfluid diluent (**d**). The illustrations (**e**) and statistical analysis (**f**) of nitenpyram release in N@UK-siRNA/DMSNs. Gel electrophoresis images exhibiting the best ratio of siRNA/PEI-DMSNs (**g**) and the stability of siRNA in N@UK-siRNA/DMSNs after exposure to air (**h**)

ultimately leading to the release of siRNA and nitenpyram [38, 39]. Therefore, N@UK-siRNA/DMSNs could significantly improve the stability of loaded RNA and had the characteristics of responding to GSH release

In order to determine the control effect of nanomaterials on *S. furcifera*, the HN-Lab and JL21 strains were treated with 0.05, 0.1, 0.25, 0.5, 1, 2, 4, and 8 μg/mL concentrations of nitenpyram and N@UK-siRNA/DMSNs for 96 h by the seed soaking method. The LC_{50} of the HN-Lab strain to N@UK-siRNA/DMSNs was 0.252 μg/mL, significantly higher than that of nitenpyram (1.353 μg/mL), with non-overlapping 95% confidence intervals, resulting in a synergistic ratio (SR) of 5.37-fold (Table 1). Similarly, the LC_{50} of the JL21 strain to N@UK-siRNA/DMSNs was 0.250 μg/mL, significantly exceeding that of nitenpyram (1.782 μg/mL), also with non-overlapping 95% confidence intervals, yielding a SR of 7.13-fold (Table 1). In comparison to pure chemical insecticides, multi-component nanobiological agents exhibited superior control efficacy under field conditions [40].

The mortality rates in the N@UK-siRNA/DMSNs treatment of the HN-Lab strain (11.1%, 31.1%, 46.7%, 71.1%, 80.0%, 88.9%, 100.0%, and 100.0%) were higher than those in the nitenpyram group (0.0%, 2.2%, 6.7%, 13.3%, 44.4%, 62.2%, 82.2%, and 95.6%), except for the 8 μg/mL nitenpyram concentration, where the difference was not statistically significant (Fig. 3a). However, for all other concentrations, the differences were statistically significant. When the JL21 strain was treated with nitenpyram and N@UK-siRNA/DMSNs at 0.25, 0.5, 1, 2, 4, and 8 μg/mL using the seed soaking method, the mortality rates in the N@UK-siRNA/DMSNs treatment group (55.6%, 64.4%, 77.8%, 91.1%, 97.8%, and 100.0%) were consistently higher than those in the nitenpyram group (2.2%, 24.4%, 42.2%, 51.1%, 57.9%, and 93.3%) (Fig. 3b). Previous studies have also shown promising results using nanocomposites carrying siRNA and insecticides. For instance, Cao et al. [41] also found that nanocomposites carrying siRNA and adriamycin exhibited high control efficacy, reducing the IC_{50} from 0.28 μM to 0.002 μM. Qu et al. [42] found that when nanomaterial SPc simultaneously loaded dsSynapsin and thiamethoxam, even at extremely low doses of thiamethoxam (1 mg/L), over 90% of cotton aphids were killed. However, Lv et al. [20] used RHMS loaded with imidacloprid and dsCYP6CY13, reducing its LC_{50} from 350.06 μg/mL to 179.79 μg/mL, with a synergistic ratio of only 1.95; this difference may be related to the different target genes selected by different authors.

Varying phenotypes were observed in the JL21 strain of *S. furcifera* after treatment with N@UK-siRNA/DMSNs at diverse concentrations (Fig. 3c, d). For instance, at a 0.25 μg/mL concentration, the insect's body tissues, including muscle fibers and epidermis, exhibited scattered blue granules, with a higher density in the dermis layer. Additionally, some neural tissues in the compound eyes displayed disintegration (Fig. 3d). With a 0.5 μg/mL concentration, blue granules were distributed across several body tissues, partial dermal cells were fragmented, and noticeable gaps emerged between the epidermis layer and internal organs, alongside a disconnection between the compound eyes and the brain (Fig. 3d). At 1.0 μg/mL, the insect's abdominal region shriveled, organs were speckled with blue granules, dermal cell membranes ruptured, and organelles and cytoplasm from different cells fused. Gradually, brain organs became undetectable (Fig. 3d). When treated with 2.0 μg/mL, the abdominal organs' shrinkage was particularly pronounced. Blue granules were present in the brain, muscles, and dermis, and significant gaps appeared between dermal cells and the epidermis layer, with some dermal cells fragmenting (Fig. 3d). Finally, at 4.0 μg/mL, the insect's body tissues dissolved, leaving no discernible tissues inside. The remaining cells were scattered throughout the body, and no dermal cell layer was observed in the epidermis layer (Fig. 3d). *USP* functions as an orphan nuclear receptor for ecdysteroids, playing critical roles in insect cell differentiation, metabolism, immune responses, and various other biological processes [43]. Therefore, when USP was knocked down, the resulting insects exhibited multiple developmental deformities. Meanwhile, *Kr-h1* has been identified in insects as the major responsive gene activated by juvenile hormone receptor, serving as a key downstream transcription factor of juvenile hormone receptor Met in metamorphosis, reproduction, cell proliferation, differentiation, and apoptosis [44]. Given the

Table 1 Toxicity of the HN-lab and JL21 strains against nitenpyram and N@UK-siRNA/DMSNs

Population	Treatment	Slope ± SE	LC_{50} μg/mL (95% CI)	χ2 (df)	*P*	SR
HN-lab	Nitenpyram	2.064 ± 0.188	1.353(1.110–1.658)	11.539(22)	0.966	–
	N@UK-siRNA/DMSNs	1.617 ± 0.151	0.252(0.195–0.320)	6.957(22)	0.999	5.37
JL21	Nitenpyram	1.663 ± 0.192	1.782(1.407–2.286)	15.154(16)	0.513	–
	N@UK-siRNA/DMSNs	1.529 ± 0.241	0.250(0.139–0.360)	6.973(16)	0.974	7.13

LC_{50} values were considered significantly different when their 95% CI did not overlap. [a] SR, synergistic ratio, calculated as LC_{50} of nitenpyram/LC_{50} of N@UK-siRNA/DMSNs. [b] Chi square value (χ^2) and degrees of freedom (df) as calculated by using Probit analysis (Polo Plus 2.0)

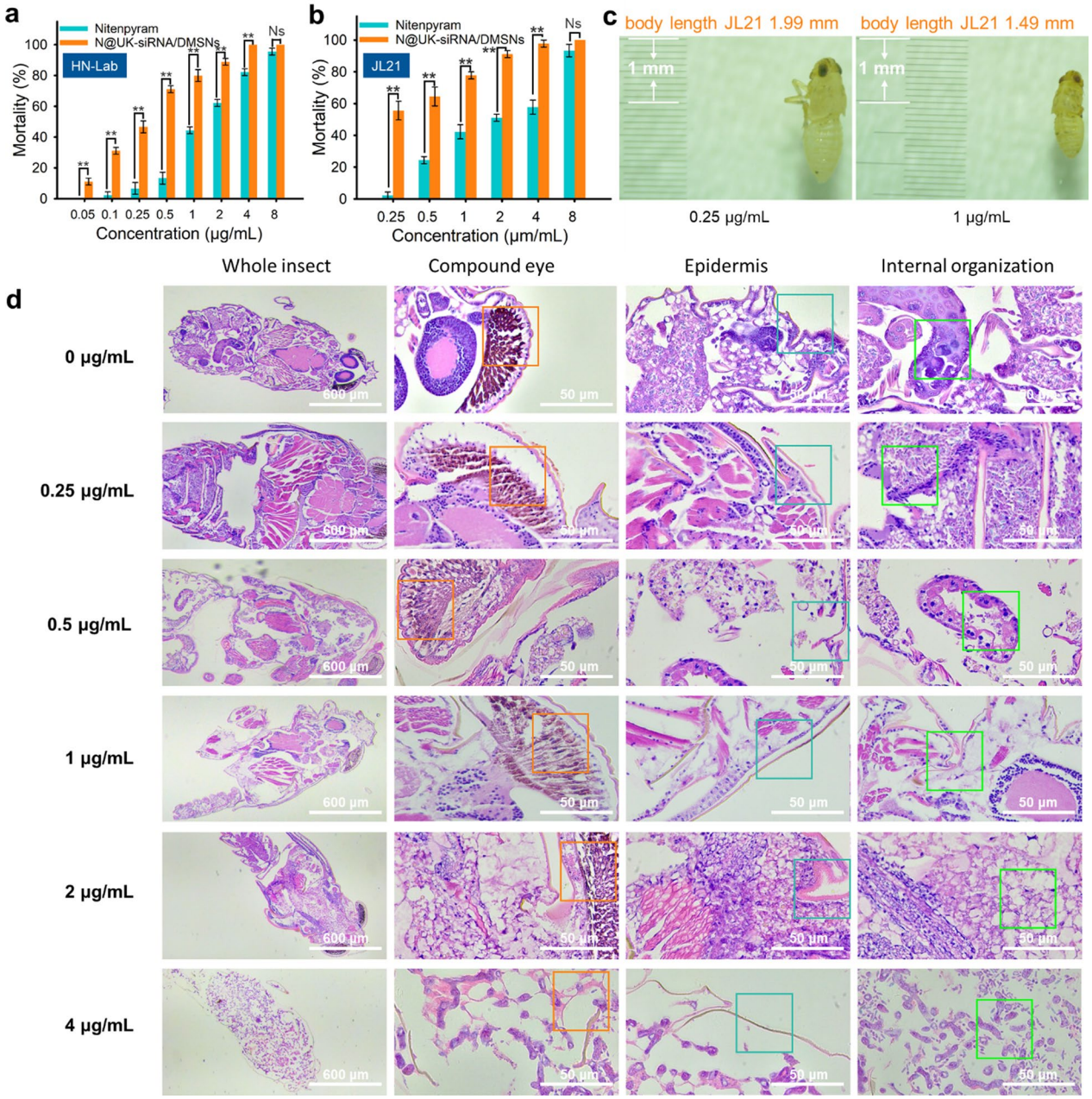

Fig. 3 The toxicity determination of N@UK-siRNA/DMSN against *S. furcifera* and its in vitro insecticidal characterization. **a**, **b** Comparison of mortality of HN-Lab and JL21 strains to N@UK-siRNA/DMSNs and nitenpyram at different concentrations. the *P*-values on the mortality of HN-Lab strain treated by 0.05, 0.1, 0.25, 0.5, 1, 2, 4, and 8 μg/mL N@UK-siRNA/DMSN were 0.007, 0.001, 0.002, 0.000, 0.001, 0.001, 0.001, and 0.116 respectively; and the *P*-values on the mortality of JL21 strain treated by different concentrations of N@UK-siRNA/DMSN were 0.001, 0.003, 0.002, 0.000, 0.001, and 0.158 respectively. **c** Photographs illustrating the impact of different concentrations of N@UK-siRNA/DMSNs on individual development of *S. furcifera*. **d** Tissue section photographs illustrating the impact of different concentrations of N@UK-siRNA/DMSNs on the tissue development of *S. furcifera*

crucial role of *USP* and *Kr-H1* in regulating the development and metabolic detoxification of *S. furcifera*, selecting these genes as targets offers significant advantages for pest resistance management.

Translocation, enrichment and biocompatibility of N@UK-siRNA/DMSN in rice

To determine the translocation and accumulation of N@UK-siRNA/DMSNs in rice, fluorescence microscopy and confocal laser scanning microscope were used to

determine the fluorescence intensity of rice seedlings and *S. furcifera*, after treated with 0.25 μg/mL FITC-labeled N@UK-siRNA/DMSNs (Fig. 4). For rice seedlings, the fluorescence intensity in the stem internode was higher when treated via leaf soaking compared to root soaking. Fluorescence accumulation was observed between and within the cell walls of the stem internode and xylem tissues, indicating bidirectional nanoparticle transfer in rice through multiple pathways (Fig. 4a, b). Similarly, in *S. furcifera*, the fluorescence intensity was greater when treated via leaf soaking versus root soaking, with accumulation observed in the epidermis layer and muscle

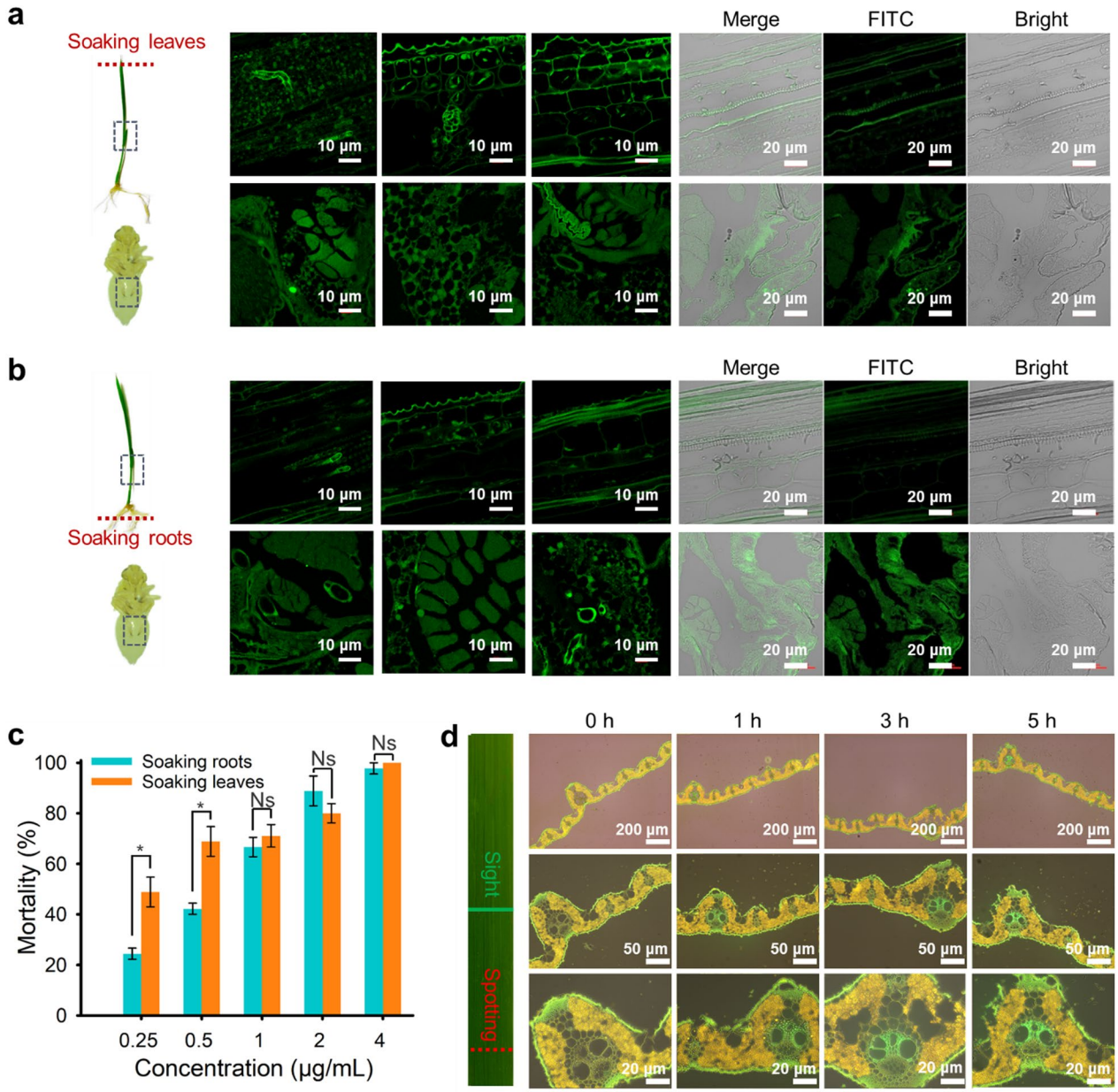

Fig. 4 Characterization of FITC-labeled N@UK-siRNA/DMSNs transport and accumulation in rice stem and *S. furcifera*. **a**, **b** Comparative analysis of the enrichment of FITC-labeled N@UK-siRNA/DMSNs within rice stems and bodies of *S. furcifera* after root soaking and leaf soaking treatments, respectively; The black dotted box in the schematic diagram indicates the position observed by the fluorescence microscope or confocal scanning microscope. **c** Comparison of mortality rates of JL21 after treatment with N@UK-siRNA/DMSNs via root soaking and leaf soaking methods at different concentrations; the *P*-values on the mortality comparison between root soaking and leaf soaking methods at 0.25, 0.5, 1, 2, and 4 μg/mL N@UK-siRNA/DMSN were 0.018, 0.013, 0.492, 0.275, and 0.374, respectively. **d** Observation of the enrichment of N@UK-siRNA/DMSNs in different tissues in the same position of rice leaves over varying observation times after treatment with 0.25 μg/mL FITC-labeled N@UK-siRNA/DMSNs

tissues (Fig. 4a, b). After 96 h of treatment with N@UK-siRNA/DMSNs using either leaf or root soaking methods, the mortality rates of JL21 at 0.25 and 0.5 μg/mL nitenpyram concentrations were significantly higher for leaf soaking (48.9% and 68.9%) compared to root soaking (24.4% and 42.2%) (Fig. 4c). However, there was no significant difference in mortality rates between treatment methods at other nitenpyram concentrations (66.7%–100.0%) (Fig. 4c). When rice leaves were treated with 0.25 μg/mL FITC-labeled N@UK-siRNA/DMSNs using the line-drawing method, the accumulation intensity in the vascular bundle increased over time at 0, 1, 3, and 5 h (Fig. 4d). This study suggests that DMSNs can mediate water transport in the plant phloem, thereby enhancing the delivery of plant-derived insecticides to target sites (vascular bundle positions) and amplifying their insecticidal effect against boring pests [45]; another study showed that foliar spray of porous hollow silica nanoparticles encapsulated with spiromesifen (average diameter of 253 nm) on plants could increase pesticide absorption and alter its transport mode [46]; SiO_2 nanoparticles could be transported from roots to aboveground parts through xylem sap [47]. The transport of nanoparticles in plants mainly occurs through two pathways: apoplastic transport and symplastic transport [48]. This study found that N@UK-siRNA/DMSNs could be transported to the vascular bundle of plants through symplastic transport, increasing the deposition of insecticide on target pests.

To test the biocompatibility of N@UK-siRNA/DMSNs with rice, rice seedlings were administered with 2.5 μg/mL of N@UK-siRNA/DMSNs, DMSNs, UK-siRNA, and nitenpyram at their two-leaf stage, and their growth parameters were evaluated after two days. The results indicated no significant variations in root length (ranging from 3.59 to 4.11 cm), plant height (7.24 to 7.68 cm), second leaf length (2.15 to 2.22 cm), and stem length (3.20 to 3.59 cm) among the groups treated with N@UK-siRNA/DMSNs, DMSNs, UK-siRNA, and nitenpyram, compared to the control group (4.00 cm, 7.12 cm, 1.96 cm, and 3.31 cm, respectively) (Fig. 5a, b). Similarly, there were no significant differences in fresh weight (0.3505 to 0.3640 g), dry weight (0.0533 to 0.0550 g), and water content (84.17 to 84.63%) between the treatment groups and the control (0.3569 g, 0.0529 g, and 85.18%, respectively) (Fig. 5c). Furthermore, the chlorophyll a (0.3783 to 0.3992 mg/g) and chlorophyll b (0.1765 to 0.1799 mg/g) content did not significantly differ between the treatment groups and the control (0.3853 mg/g for chlorophyll a)

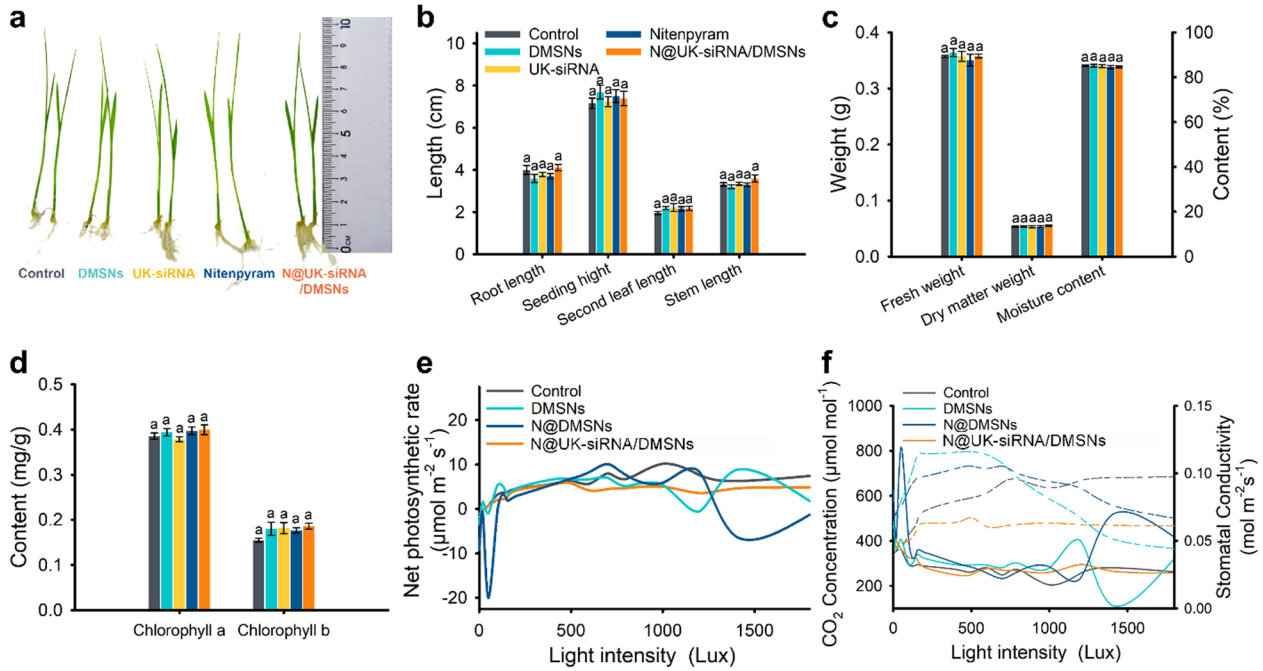

Fig. 5 Biocompatibility of N@UK-siRNA/DMSNs in rice. **a** Picture displaying the impact of 2.5 μg/mL DMSNs, UK-siRNA, nitenpyram, and N@UK-siRNA/DMSNs on rice growth and development. **b** Cartogram displaying the impact of 2.5 μg/mL N@UK-siRNA/DMSNs and its controls on rice growth and development, consisting of root length (*P*, 0.160), seeding height (*P*, 0.733), second leaf length (*P*, 0.519), and stem length (*P*, 0.114). **c** Influence of N@UK-siRNA/DMSNs and its controls on rice fresh weight (*P*, 0.771), dry matter weight (*P*, 0.854), and moisture content (*P*, 0.886). **d** Effects of N@UK-siRNA/DMSNs and its controls on the content of chlorophyll a (*P*, 0.444) and chlorophyll b (*P*, 0.126) in rice. **e**, **f** Photosynthesis determination exhibiting the effects of nanomaterials DMSNs, N@DMSNs, and N@UK-siRNA/DMSNs on the net photosynthetic rate, intercellular CO_2 concentrations and stomatal conductivity in rice

(Fig. 5d). The results of nanoparticles on rice photosynthesis showed that the effects of N@UK-siRNA/DMSNs, DMSNs, and N@DMSNs on the net photosynthetic rate and intercellular CO2 concentrations in rice leaves were not obvious, under different light intensities; however, its stomatal conductivity treated with N@UK-siRNA/DMSNs was consistently lower than that of the control treatment (Fig. 5e). This led to a decrease in stomatal conductance under strong light (Fig. 5e), resulting in significant changes in intercellular CO_2 concentration and net photosynthetic rate (Fig. 5f). Compared to DMSNs and N@DMSNs, N@UK-siRNA/DMSNs with positive charges exhibited higher cellular compatibility, resulting in similar intracellular CO_2 concentrations and net photosynthesis as the control (Fig. 5e, f), with minimal fluctuations under varying light intensities. The effects of nanoparticles on plants can vary, with some studies reporting positive outcomes, while others demonstrate negative or negligible impacts. For instance, Khodakovskaya et al. [49] reported an increase in germination rate of tomato seeds from 71 to 90% when treated with multi-walled carbon nanotubes compared to the control group. Some studies indicate that silicon dioxide nanoparticles significantly reduce plant height and biomass of both above-ground and root parts [47], while others suggest positive effects on seedlings' length, root length, fresh weight, and dry weight [50]. This study concludes that N@UK-siRNA/DMSNs, DMSNs, UK-siRNA, and nitenpyram did not significantly affect the measured parameters of rice plants.

Molecular mechanism of N@UK-siRNA/DMSNs improving the sensitivity of *S. furcifera* to nitenpyram

The pymetrozine-resistant strain JL21, after feeding on 0.25 μg/mL N@UK-siRNA/DMSNs or nitenpyram using leaf-soaking method for 24 and 48 h, showed a significant decrease in the relative expression of *USP* and *Kr-H1* (0.217-fold and 0.284-fold, 0.090-fold and 0.437-fold, respectively) in the N@UK-siRNA/DMSNs treatment compared to the nitenpyram treatment (Fig. 6b, c). After 24 h of treatment, the relative expression of detoxification metabolic genes *CYP6FJ3* and *SfABCH4* in the N@UK-siRNA/DMSNs treatment group (0.367-fold and 0.016-fold) were significantly lower than those in the nitenpyram treatment, while the relative expression of *CYP6CS3* (1.422-fold) showed no significant difference between the two treatment groups (Fig. 6e). After 48 h of treatment, the relative expression of detoxification metabolic genes *CYP6FJ3* and *SfABCH4* in the N@UK-siRNA/DMSNs treatment group (0.407-fold and 0.028-fold) were significantly lower than those in the imidacloprid treatment group, while *CYP6CS3* (1.088-fold) showed no significant difference between the two treatment groups (Fig. 6f). Additionally, the study indicated that the overexpression of the P450 gene *CYP6ER1* in *N. lugen* also contributed to the accumulation of nitenpyram resistance [51, 52]. FAM, CY3 and FITC-labeled fluorescence in situ hybridization results showed that the mRNA content of *USP* (Fig. 6a), *Kr-H1* (Fig. 6a) and *SfABCH4* (Fig. 6d) in the N@UK-siRNA/DMSNs treatment group were significantly lower than those in the nitenpyram treatment group in various tissues [7]. The results of ELISA determination showed that the SfABCH4 protein level in the dsGFP (64.07 ng/g) was significantly higher than that in the dsUSP (13.03 ng/g) and dsKr-H1 (20.05 ng/g), while the SfABCH4 protein level in the N@UK-siRNA/DMSNs group (19.50 ng/g) was significantly lower than that in the nitenpyram group (77.32 ng/g) (Fig. S7). In the tissues such as the dermis, the fluorescence intensity in the N@UK-siRNA/DMSNs group was higher than that in the nitenpyram group, indicating that the SfABCH4 protein level was significantly lower in the nitenpyram group (Fig. S8). Therefore, N@UK-siRNA/DMSNs nanoparticles not only inhibit pest growth and development but also increase the sensitivity of target pests to insecticides by suppressing the expression of detoxification genes such as *CYP6FJ3* and *SfABCH4*.

In order to explore how USP and Kr-H1 regulate detoxification genes and mediate the sensitivity of *S. furcifera* to nitenpyram, the 4th instar nymphs of JL21 were injected with dsKr-H1 or dsUSP, and the relative expression of *USP*, *Kr-H1*, and ABC genes were determined. The results showed that after 24 h, 48 h, and 72 h of dsKr-H1 interference (with relative expression of *Kr-H1* decreasing to 0.056, 0.099, and 0.021-fold, respectively), the relative expression of *USP* significantly decreased, with dropping to 0.978, 0.488, and 0.231-fold, respectively (Fig. 7a). Correspondingly, the relative expression of *SfABCH4* decreased to 0.552, 0.524, and 0.023-fold, respectively, and *Sfur003381.1* decreased to 0.091, 0.120, and 0.737-fold, respectively. After 24 h, 48 h, and 72 h of dsUSP interference (with relative expression of *USP* decreasing to 0.287, 0.311, and 0.478-fold, respectively), the relative expression of *Kr-H1* significantly decreased, with dropping to 0.056, 0.715, and 0.052-fold, respectively (Fig. 7a). Correspondingly, the relative expression of *SfABCH4* decreased to 0.564, 0.309, and 0.029-fold, respectively, and *Sfur003381.1* decreased to 0.558, 0.600, and 0.048-fold, respectively (Fig. 7a). The expression trends of *SfABCH4*, *Sfur003381.1*, *Kr-H1*, and *USP* were consistent and clustered into one category, with *SfABCH4* showing a greater decrease in relative expression (Fig. 7a). The mechanisms underlying pest resistance primarily involve an enhanced activity of detoxification enzymes (including ABC, etc.) [53]. Therefore, *Kr-H1* or *USP* may be involved in the transcriptional regulation of

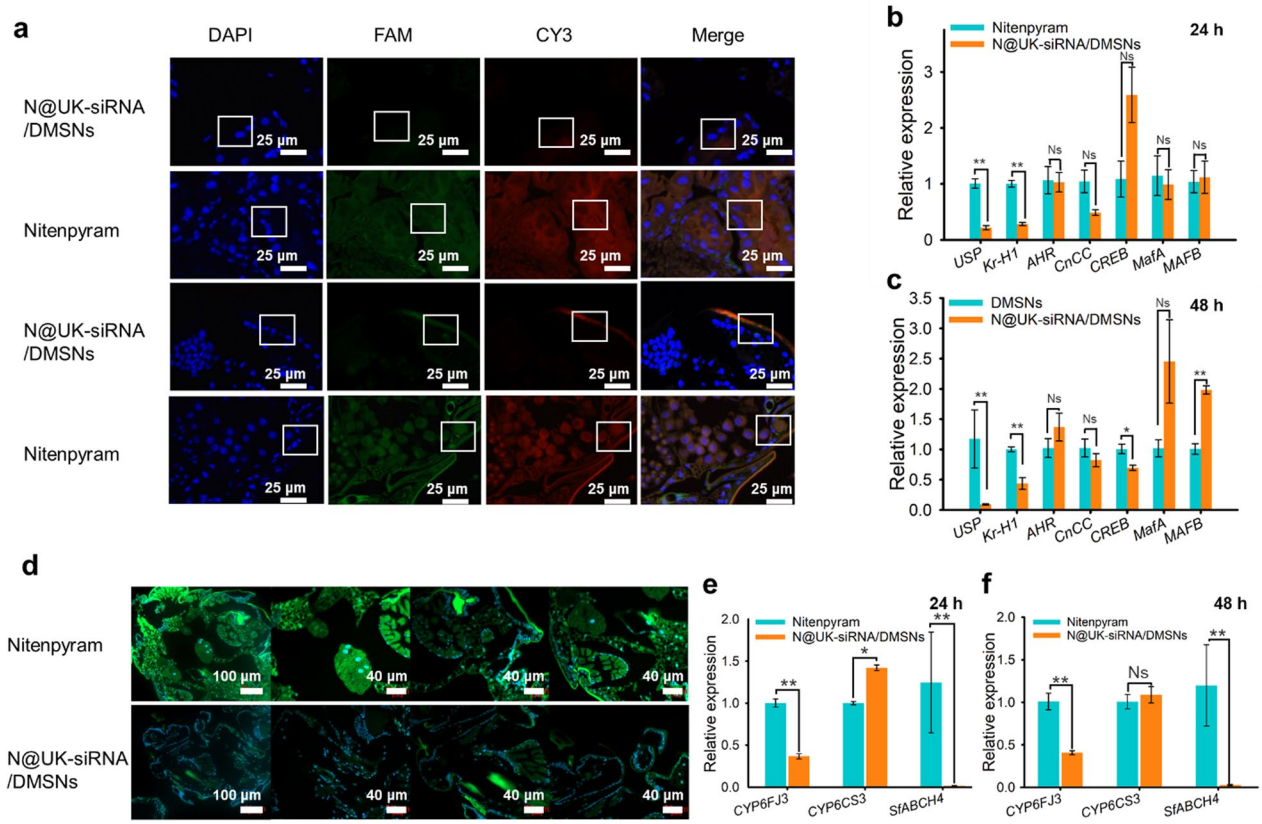

Fig. 6 N@UK-siRNA/DMSNs downregulating the developmental genes *USP* and *Kr-H1*, and detoxification genes ABCs *SfABCH4* and P450s *CYP6FJ3*, enhancing the sensitivity of *S. furcifera* to nitenpyram. **a** Fluorescence in situ hybridization assay characterizing changes of the *USP* and *Kr-H1* expression after feeding on N@UK-siRNA/DMSNs or nitenpyram. **b**, **c** Relative expression changes of transcription factors *AHR*, *CnCC*, *CREB*, *MafA*, *USP*, or *Kr-H1* genes after feeding on 0.25 μg/mL N@UK-siRNA/DMSNs or nitenpyram for 24 (their *P*-values were 0.908, 0.055, 0.064, 0.739, 0.834, 0.001 and 0.000 respectively) and 48 h (their *P*-values were 0.284, 0.332, 0.025, 0.111, 0.001, 0.008 and 0.006 respectively). **d** Fluorescence in situ hybridization assay characterizing changes of the *SfABCH4* expression after feeding on different treatment. **e**, **f** Changes in relative expression of detoxification metabolic genes *CYP6FJ3*, *CYP6CS3*, and *SfABCH4* after N@UK-siRNA/DMSNs or nitenpyram treatment; their *P*-values at 24 h 0.000, 0.011, and 0.001 respectively; and their *P*-values at 48 h 0.004, 0.562, and 0.009 respectively

SfABCH4 [54], to involve in regulating the sensitivity of *S. furcifera* to nitenpyram. In insects, *USP*, as a homologous gene of the class of retinoid X receptor *RXR* [55], plays a key role in regulating metabolic detoxification genes and development processes after stimulation by corresponding exogenous or endogenous compounds [56], including but not limited to *ABCA1* [57]. Yeast one-hybrid assays showed that on triple-dropout medium containing 50 mM 3-AT, the growth trend of yeast co-transformed with pHis2-SfABCH4p and pGADT7-USP or pHis2-SfABCH4p and pGADT7-Kr-H1 was significantly better than that of yeast co-transformed with pHis2-SfABCH4p and pGADT7 (Fig. 7b). At concentrations of 0, 0.5, and 1 μg/mL of nitenpyram, the mortality rates of the *S. furcifera* in the dsUSP & dsKr-H1 (44.4%–100.0%), dsUSP (51.1%–100.0%), and dsKr-H1 (51.1%–100.0%) treatment

(See figure on next page.)

Fig. 7 Molecular mechanism of *USP* and *Kr-H1* regulating detoxification genes. **a** Relative expression changes of *USP*, *Kr-H1*, and different ABCs genes after silencing *USP* or *Kr-H1* at 24, 48, and 72 h. **b** Yeast one-hybrid assay testing the binding activity of *USP* or *Kr-H1* to the *SfABCH4* gene promoter. **c** Changes in sensitivity of *S. furcifera* to 0 (*P*, 0.001), 0.5 (*P*, 0.000), and 1 (*P*, 0.000) μg/mL of nitenpyram after silencing *USP* or *Kr-H1*. **d** Molecular docking assay testing the binding activity of SfABCH4 to nitenpyram, the analysis of the binding sites of SfABCH4 and nitenpyram on the left, and analysis of the binding modes of SfABCH4 and nitenpyram on the right. **e**, **f** The affinity of SfABCH4 protein and nitenpyram was verified by isothermal titration calorimetry, **e** depicting the real-time process of the heat change rate nitenpyram titrating in SfABCH4, while **f** illustrating the enthalpy and its fitted curve for each titration of nitenpyram in SfABCH4

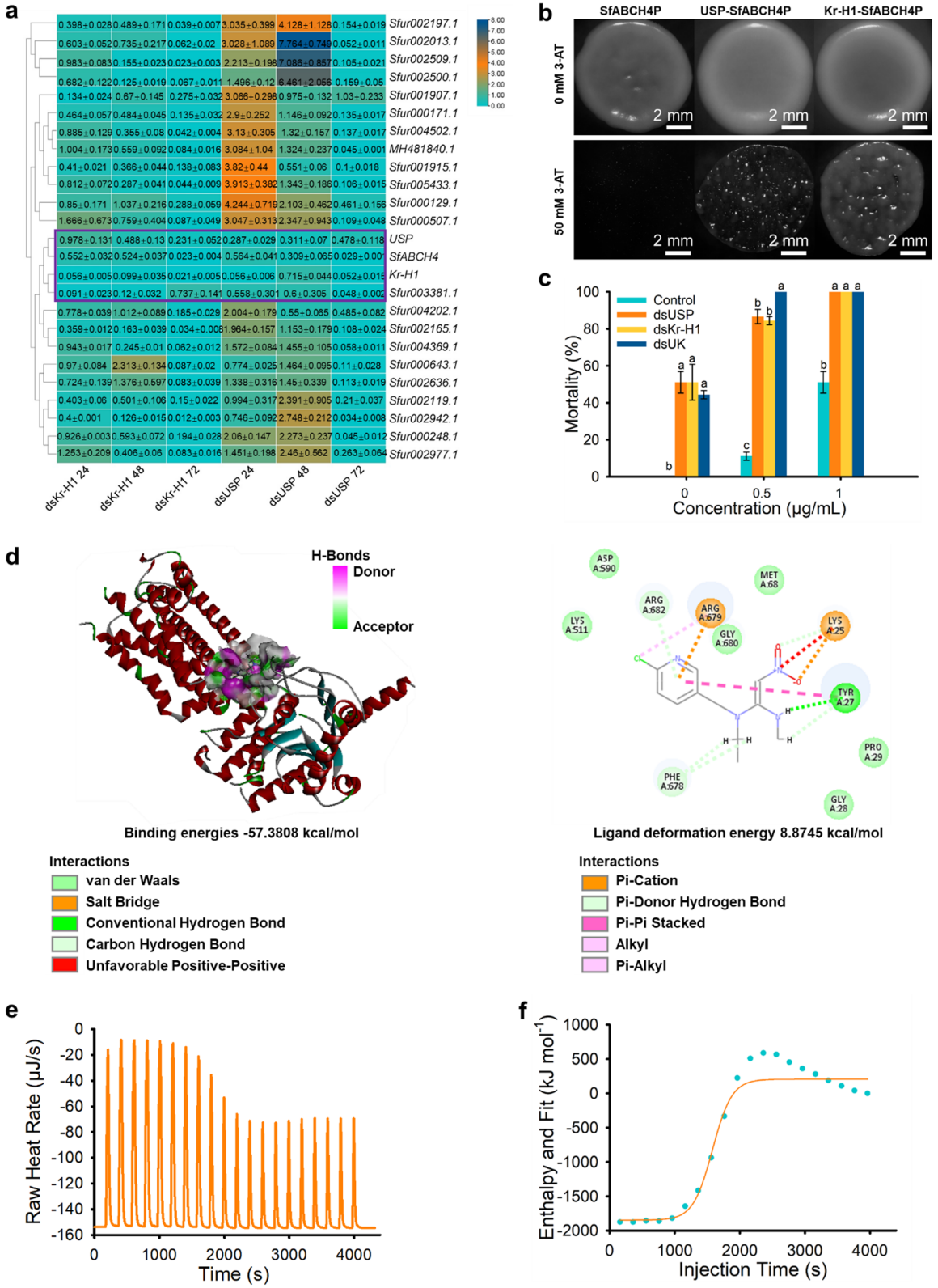

Fig. 7 (See legend on previous page.)

groups were significantly higher than those in the dsGFP treatment group, and at a concentration of 0.5 μg/mL nitenpyram, the mortality rate in the dsUSP & dsKr-H1 treatment group (100.0%) was significantly higher than that in the dsUSP (86.7%) and dsKr-H1 (84.4%) treatment groups (Fig. 7c). Therefore, USP or Kr-H1 can regulate the expression of detoxification genes such as *SfABCH4* [58]. Molecular docking experiments showed that the binding energies between the SfABCH4 protein and nitenpyram molecules were −57.3808 kcal/mol, and the ligand deformation energy was 8.8745 kcal/mol (Fig. 7d–f). In SfABCH4, there were 11 amino acid residues that interacted with nitenpyram through van der Waals forces, salt bridge, hydrogen bond, Pi-Pi Stacked, etc.; TYR27, PHE678, and ARG682 formed hydrogen bonds directly with the amino or pyridine ring of nitenpyram; ARG679, LYS25 formed pi bonds with nitenpyram, etc. (Fig. 7d, e). Isothermal titration calorimetry confirmed that the SfABCH4 protein exhibits high affinity for nitenpyram (Fig. 7e, f). Studies have shown that the expression level of *NlABCG3* in *Nilaparvata lugen* was significantly positively correlated with resistance to nitenpyram, and silencing *NlABCG3* significantly increases the sensitivity of *N. lugen* to nitenpyram [59]. Overexpression of metabolic detoxification genes plays a crucial role in enhancing resistance by increasing the expression of metabolic resistance genes, such as ABC *SfABCH4* [60]. The overexpression of metabolic detoxification genes is typically regulated by transcription factors such as *USP* [61, 62]. Therefore, *USP* or *Kr-H1* can participate in the detoxification process of nitenpyram and other insecticides by regulating detoxification genes such as *SfABCH4* (Fig. S5), thereby increasing its sensitivity to nitenpyram.

In this study, two transcription factors that could regulate metabolic detoxification were identified by revealing the resistance mechanisms of *S. furcifera* and analyzing its detoxification processes. The knockdown of these transcription factors with siRNA had proven effective in managing the resistance. Currently, utilizing transcriptional regulatory factors for integrated pest management and resistance control shows significant potential. In addition to the transcription factors *USP* and *Kr-H1* identified in this study, *cAMP-response element-binding protein* [63], *aryl hydrocarbon receptor* [64], and *cap 'n' collar isoform C* [65] have also been confirmed to modulate metabolic detoxification genes, influencing pest sensitivity to chemical pesticides. Our study focuses on using DMSNs to deliver siRNA for the control of *S. furcifera*, but research has indicated that combining nanotechnology with RNA interference (RNAi) to create sprayable nucleic acid nanopesticides offered advantages such as high specificity [66], no residues, and minimal impact on non-target organisms, making it a hotspot in the development of novel green pesticides. In addition to our findings, loading siRNA into layered double hydroxide clay nanosheets [67], chitosan [68], carbon-based materials [69], liposomes [70], or star-shaped polycations [71] has also been shown to delay pest development and increase mortality rates. To the best of our knowledge, DMSNs demonstrates significant advantages in synthetic processes, enhancing RNA stability, RNA trafficking and improving control efficacy [72]. Therefore, the delivery system of RNAi pesticides loaded in DMSNs holds great potential for the prevention and control of crop pests and diseases.

Conclusion

RNAi insecticides are considered as a potentially efficient strategy for preventing *S. furcifera* that poses a growing threat to rice production, due to the escalating resistance of *S. furcifera* to various insecticides. In this research, we have recognized two key challenges: (i) the instability of siRNA with the low residual concentration in insect bodies and (ii) the low efficiency of siRNA delivery from crops to target pests. With the characterization of high specific surface area, biocompatibility and efficiency of cellular internalization, DMSNs allows symplastic and apoplastic pathways via the phloem and xylem tissues. Here, the N@UK-siRNA/DMSNs with loading nitenpyram with a loading rate of 20.3% and UK-siRNA were designed as the delivery carriers, which significantly enhanced the stability of UK-siRNA for 21 days. By enriching on the feeding sites of *S. furcifera*, the prepared N@UK-siRNA/DMSNs increased the sensitivity of test insects to nitenpyram with an enhancement ratio ranging from 5.37–7.13 (including the susceptible strain HN-Lab and the resistant strain JL21), which achieved negligible adverse effects on rice and made it suitable for managing resistance in *S. furcifera*. The maximum release rate of loading nitenpyram reached 84.99%, and the released UK-siRNA significantly downregulates the developmental genes *USP* and *Kr-H1*, as well as the downstream detoxification genes ABC *SfABCH4* and P450 *CYP6FJ3*. *SfABCH4* enhances sensitivity to nitenpyram by mediating its efflux, thus increasing susceptibility to nitenpyram. Together, this DMSNs-delivered RNAi insecticides enhance control efficiency against *S. furcifera* and thus hold considerable promise for ensuring the green and safe production of rice.

Supplementary Information

The online version contains supplementary material available at https://doi.org/10.1186/s12951-024-02966-8.

Supplementary Material 1.

Acknowledgements
We are particularly grateful to Chengdu Baichuang Technology Co., Ltd. (Chengdu, China) for its help in the purchase of reagents and compounds. This research is financially supported by the state key laboratory of crop gene exploration and utilization in southwest China (SKL-ZY202221). The authors acknowledge support from the National Natural Science Foundation of China (Grant No. 22202049) and Science & Technology Department of Sichuan Province (Grant No. 2024NSFSC1186, 2024ZYD0127).

Author contributions
Xuegui Wang: designed the research, polished and revised the manuscript. Changwei Gong: performed the assays, analyzed the data, and wrote the manuscript. Wei Wang: analyzed the data, polished and revised the manuscript. Yanxin Ma: analyzed the data and performed some assays. Xiaoxu Zhan: performed some assays, polished and revised the manuscript, and analyzed the data. Anchun Peng: improved experimental design. Jian Pu: revised the manuscript. Jizhi Yang: revised the manuscript, and raised some valuable suggestions for the pictures and experimental methods.

Data availability
No datasets were generated or analysed during the current study.

Declarations

Competing interests
The authors declare no competing interests.

Author details
[1]State Key Laboratory of Crop Gene Exploration and Utilization in Southwest China, Sichuan Agricultural University, Chengdu 611130, China. [2]College of Agriculture, Sichuan Agricultural University, Chengdu 611130, China. [3]College of Science, Sichuan Agricultural University, Chengdu 611130, China. [4]Institute of Urban Agriculture, Chinese Academy of Agricultural Sciences, Chengdu 611130, China.

Received: 1 August 2024 Accepted: 31 October 2024
Published online: 27 November 2024

References

1. Wang WW, Zhou PY, Mo XC, Hu LF, Jin N, Chen X, Yu ZX, Meng JP, Erb M, Shang ZC, et al. Induction of defense in cereals by 4-fluorophenoxyacetic acid suppresses insect pest populations and increases crop yields in the field. Proc Natl Acad Sci USA. 2020;117:12017.
2. Wang L, Tang N, Gao XL, Chang ZX, Zhang LQ, Zhou GH, Guo DY, Zeng Z, Li WJ, Akinyemi IA, et al. Genome sequence of a rice pest, the white-backed planthopper (*Sogatella furcifera*). Gigascience. 2017;6:9.
3. Zhou GH, Wen JJ, Cai DJ, Li P, Xu DL, Zhang SG. Southern rice black-streaked dwarf virus: a new proposed *Fijivirus* species in the family *Reoviridae*. Chin Sci Bull. 2008;53:3677.
4. Guo H, Long GJ, Liu XZ, Ma YF, Zhang MQ, Gong LL, Dewer Y, Hull JJ, Wang MM, Wang Q, et al. Functional characterization of tyrosine melanin genes in the white-backed planthopper and utilization of a spray-based nanoparticle-wrapped dsRNA technique for pest control. Int J Biol Macromol. 2023;230: 123123.
5. Mao KK, Ren ZJ, Li WH, Liu CY, Xu PF, He S, Li JH, Wan H. An insecticide resistance diagnostic kit for whitebacked planthopper *Sogatella furcifera* (Horvath). J Pest Sci. 2021;94:531.
6. Hites RA. The rise and fall of chlorpyrifos in the United States. Environ Sci Technol. 2021;55:1354.
7. Du Q, Ding X-Q, Gao F, Cui B, Wang T-Y, Chen F-Y, Chen L, Chen H-Y, Cui H-X, Wang Y. Thermo-responsive liposome nano-vesicles for co-delivery of emamectin benzoate and nitenpyram with synergistic pest control. Chem Eng J. 2024;479: 147548.
8. Liang XM, Guan FL, Ling ZY, Wang HH, Tao YW, Kraka E, Huang HJ, Yu CL, Li DP, He JB, Fang HS. Pivotal role of water molecules in the photodegradation of pymetrozine: new insights for developing green pesticides. J Hazard Mater. 2022;423: 127197.
9. Wu JC, Ge LQ, Liu F, Song QS, Stanley D. Pesticide-induced planthopper population resurgence in rice cropping systems. Annu Rev Entomol. 2020;65:409.
10. Chen XM. Small RNAs and their roles in plant development. Annu Rev Cell Dev Biol. 2009;25:21.
11. Gutbrod MJ, Martienssen RA. Conserved chromosomal functions of RNA interference. Nat Rev Genet. 2020;21:311.
12. Jadhav V, Vaishnaw A, Fitzgerald K, Maier MA. RNA interference in the era of nucleic acid therapeutics. Nat Biotechnol. 2024;42:394.
13. Raman P, Zaghab SM, Traver EC, Jose AM. The double-stranded RNA binding protein RDE-4 can act cell autonomously during feeding RNAi in *C. elegans*. Nucleic Acids Res. 2017;45:8463.
14. Castellanos NL, Smagghe G, Taning CNT, Oliveira EE, Christiaens O. Risk assessment of RNAi-based pesticides to non-target organisms: evaluating the effects of sequence similarity in the parasitoid wasp. Sci Total Environ. 2022;832: 154746.
15. Fletcher SJ, Reeves PT, Hoang BT, Mitter N. A perspective on RNAi-based biopesticides. Front Plant Sci. 2020;11:51.
16. Parker KM, Borrero VB, van Leeuwen DM, Lever MA, Mateescu B, Sander M. Environmental fate of rna interference pesticides: adsorption and degradation of double-stranded rna molecules in agricultural soils. Environ Sci Technol. 2019;53:3027.
17. Wang M, Jin HL. Spray-induced gene silencing: a powerful innovative strategy for crop protection. Trends Microbiol. 2017;25:4.
18. Wang M, Weiberg A, Lin FM, Thomma BPHJ, Huang HD, Jin HL. Bidirectional cross-kingdom RNAi and fungal uptake of external RNAs confer plant protection. Nat Plants. 2016;2:16151.
19. Zhao JH, Guo HS. RNA silencing: from discovery and elucidation to application and perspectives. J Integr Plant Biol. 2022;64:476.
20. Lv HX, Li XC, Li JQ, Yu C, Zeng QH, Ning GG, Wan H, Li JH, Ma KS, He S. Overcoming resistance in insect pest with a nanoparticle-mediated dsRNA and insecticide co-delivery system. Chem Eng J. 2023;475: 146239.
21. Zhang ZL, Wanga XJ, Lua JB, Bin Lua H, Yea ZX, Xua ZT, Zhang C, Chen JP, Li JM, Zhang CX, Huang HJ. Cross-kingdom RNA interference mediated by insect salivary microRNAs may suppress plant immunity. Proc Natl Acad Sci USA. 2024;121: e2318783121.
22. Wang YX, Li MS, Ying JH, Shen J, Dou DL, Yin MZ, Whisson SC, Birch PRJ, Yan S, Wang XD. High-efficiency green management of potato late blight by a self-assembled multicomponent nano-bioprotectant. Nat Commun. 2023;14:5622.
23. Fu LH, Wan YL, Qi C, He J, Li CY, Yang C, Xu H, Lin J, Huang P. Nanocatalytic theranostics with glutathione depletion and enhanced reactive oxygen species generation for efficient cancer therapy. Adv Mater. 2021;33:2006892.
24. Gong CW, Wang XG, Huang Q, Zhang JY, Zhang YM, Zhan XX, Zhang SR, Hasnain A, Ruan YW, Shen LT. The fitness advantages of bistrifluron resistance related to chitin synthase A in *Spodoptera litura* (Fab.) (Noctuidae: Lepidoptera). Pest Manag Sci. 2021;77:3458.
25. Zhang YM, Ruan YW, Gong CW, Zhang SR, Zhang JY, He YF, Wang QL, Liu D, Pu J, Liu XM, et al. Reproductive outbreaks of *Sogatella furcifera* mediated by overexpression of the nuclear receptor *USP* under pressure from triflumezopyrim. Int J Mol Sci. 2022;23:13769.
26. Wang K, Wang Y, Wu YY, Jiang JJ, Zhang YX, Yu N, Liu ZW. A novel dual stimuli-responsive and double-loaded insecticidal nanoformulation for efficient control of insect pest. Chem Eng J. 2023;474: 146012.
27. Xu C, Lei C, Wang Y, Yu CZ. Dendritic mesoporous nanoparticles: structure, synthesis and properties. Angewandte Chemie-International Edition. 2022;61: e202112752.
28. Kienzle A, Kurch S, Schlöder J, Berges C, Ose R, Schupp J, Tuettenberg A, Weiss H, Schultze J, Winzen S, et al. Dendritic mesoporous silica nanoparticles for pH-stimuli-responsive drug delivery of TNF-alpha. Adv Healthc Mater. 2017;6:1700012.

29. Deng C, Liu YH, Zhou FZ, Wu MY, Zhang Q, Yi DL, Yuan W, Wang YJ. Engineering of dendritic mesoporous silica nanoparticles for efficient delivery of water-insoluble paclitaxel in cancer therapy. J Colloid Interface Sci. 2021;593:424.
30. Lee JY, Kim MK, Nguyen TL, Kim J. Hollow mesoporous silica nanoparticles with extra-large mesopores for enhanced cancer vaccine. ACS Appl Mater Interfaces. 2020;12:34658.
31. Solymosi F, Novak E, Molnar A. Infrared spectroscopic study on carbon monoxide-induced structural changes of iridium on an alumina support. J Phys Chem. 1990;94:7250.
32. Shen YF, Suib SL, Deeba M, Koermer G. Luminescence and IR characterization of acid sites on alumina. J Catal. 1994;146:483–90.
33. Wang S, Liu S, Zhang J, Cao Y. Highly fluorescent nitrogen-doped carbon dots for the determination and the differentiation of the rare earth element ions. Talanta. 2019;198:501–9.
34. Li KR, Li BD, Li X. A novel material poly(N-acryloyl-L-glycine)-brush grafted N-doped magnetic biochar by surface-initiated RAFT polymerization for efficient elimination of heavy metal ions. Sep Purif Technol. 2022;292: 121053.
35. Mai L, Lam T, Bui Q, Nhac-Vu H-T. Efficient hydrogen evolution reaction in alkaline via novel hybrid of Pt deposited zinc phosphide nanosheets. Mater Res Bull. 2021;133: 111024.
36. Hsiao Y-S, Chen P-M, Khung YL. Thermal reactivity of pyrrole and its methyl derivatives on silicon (111) hydride surfaces. Appl Surf Sci. 2023;613: 156005.
37. Dong Y, Fang XP, Yang Y, Xue GP, Chen X, Zhang WL, Wang XM, Yu CL, Zhou J, Mei Q, et al. Comparative proteomic analysis of susceptible and resistant rice plants during early infestation by small brown planthopper. Front Plant Sci. 2017;8:1744.
38. Li J, Tian H, Zhu F, Jiang S, He M, Li Y, Luo Q, Sun W, Liu XL, Wang P. Amorphous ultra-small fe-based nanocluster engineered and ICG loaded organo-mesoporous silica for GSH depletion and photothermal-chemodynamic synergistic therapy. Adv Healthc Mater. 2022;11:2201986.
39. Yang Y, Wan J, Niu Y, Gu Z, Zhang J, Yu M, Yu C. Structure-dependent and glutathione-responsive biodegradable dendritic mesoporous organosilica nanoparticles for safe protein delivery. Chem Mater. 2016;28:9008–16.
40. Ha M, Kim J-H, You M, Li Q, Fan C, Nam J-M. Multicomponent plasmonic nanoparticles: from heterostructured nanoparticles to colloidal composite nanostructures. Chem Rev. 2019;119:12208–78.
41. Cao N, Cheng D, Zou SY, Ai H, Gao JM, Shuai XT. The synergistic effect of hierarchical assemblies of siRNA and chemotherapeutic drugs co-delivered into hepatic cancer cells. Biomaterials. 2011;32:2222.
42. Qu XT, Wang SJ, Lin GZ, Li MS, Shen J, Wang D. The Synergistic effect of thiamethoxam and synapsin dsRNA targets neurotransmission to induce mortality in *Aphis gossypii*. Int J Mol Sci. 2022;23:9388.
43. Ruan ZR, Yu Z, Xing C, Chen EH. Inter-organ steroid hormone signaling promotes myoblast fusion via direct transcriptional regulation of a single key effector gene. Curr Biol. 2024;34:1438.
44. Tang Y, Wu S, He HL, Gao Q, Ding WB, Xue J, Qiu L, Li YZ. The CsmiR1579-CsKr-h1 module mediates rice stem borer development and reproduction: an effective target for transgenic insect-resistant rice. Int J Biol Macromol. 2024;254: 127752.
45. Ding Z, Wei K, Zhang Y, Ma X, Yang L, Zhang W, Liu H, Jia C, Shen W, Ma S. "One-Pot" method preparation of dendritic mesoporous silica-loaded matrine nanopesticide for noninvasive administration control of *Monochamus alternatus*: the vector insect of *Bursapherenchus xylophophilus*. ACS Biomater Sci Eng. 2024;10:1507.
46. Bueno V, Gao X, Abdul Rahim A, Wang P, Bayen S, Ghoshal S. Uptake and translocation of a silica nanocarrier and an encapsulated organic pesticide following foliar application in tomato plants. Environ Sci Technol. 2022;56:6722.
47. Le VN, Rui YK, Gui X, Li XG, Liu ST, Han YN. Uptake, transport, distribution and Bio-effects of SiO_2 nanoparticles in Bt-transgenic cotton. J Nanobiotechnol. 2014;12:50.
48. Zhang HY, Su WH. Classification, uptake, translocation, and detection methods of nanoparticles in crop plants: a review. Environ Sci Nano. 1847;2024:11.
49. Khodakovskaya M, Dervishi E, Mahmood M, Xu Y, Li Z, Watanabe F, Biris AS. Carbon nanotubes are able to penetrate plant seed coat and dramatically affect seed germination and plant growth. ACS Nano. 2009;3:3221.
50. Chourasiya V, Nehra A, Shukla P, Singh K, Singh P. Impact of mesoporous nano-silica (SiO_2) on seed germination and seedling growth of wheat, pea and mustard seed. J Nanosci Nanotechnol. 2021;21:3566.
51. Mao K, Jin R, Ren Z, Zhang J, Li Z, He S, Ma K, Wan H, Li J. miRNAs targeting *CYP6ER1* and *CarE1* are involved in nitenpyram resistance in *Nilaparvata lugens*. Insect Science. 2022;29:177.
52. Mao K, Zhang X, Ali E, Liao X, Jin R, Ren Z, Wan H, Li J. Characterization of nitenpyram resistance in *Nilaparvata lugens* (Stål). Pestic Biochem Physiol. 2019;157:26.
53. Nauen R, Bass C, Feyereisen R, Vontas J. The role of cytochrome P450s in insect toxicology and resistance. Annu Rev Entomol. 2022;67:105.
54. Li S, Zhu SM, Jia QQ, Yuan DW, Ren CH, Li K, Liu SN, Cui YY, Zhao HG, Cao YH, et al. The genomic and functional landscapes of developmental plasticity in the American cockroach. Nat Commun. 2018;9:1008.
55. Wang QQ, Miao JJ, Zhao AR, Wu MN, Pan LQ. Use of GAL4 factor-based yeast assay to quantify the effects of xenobiotics on RXR homodimer and RXR/PPAR heterodimer in scallop. Sci Total Environ. 2022;852: 158526.
56. Evans RM, Mangelsdorf DJ. Nuclear receptors, RXR, and the big bang. Cell. 2014;157:255.
57. Murthy S, Born E, Mathur SN, Field FJ. LXR/RXR activation enhances basolateral efflux of cholesterol in CaCo-2 cells. J Lipid Res. 2002;43:1054.
58. Jin M, Liu B, Zheng W, Liu C, Liu Z, He Y, Li X, Wu C, Wang P, Liu K. Chromosome-level genome of black cutworm provides novel insights into polyphagy and seasonal migration in insects. BMC Biol. 2023;21:2.
59. Li Z, Mao K, Jin R, Cai T, Qin Y, Zhang Y, He S, Ma K, Wan H, Ren X. miRNA novel_268 targeting *NlABCG3* is involved in nitenpyram and clothianidin resistance in *Nilaparvata lugens*. Int J Biol Macromol. 2022;217:615.
60. Rane RV, Walsh TK, Pearce SL, Jermiin LS, Gordon KHJ, Richards S, Oakeshott JG. Are feeding preferences and insecticide resistance associated with the size of detoxifying enzyme families in insect herbivores? Curr Opin Insect Sci. 2016;13:70.
61. Amezian D, Nauen R, Le Goff G. Transcriptional regulation of xenobiotic detoxification genes in insects-an overview. Pestic Biochem Physiol. 2021;174: 104822.
62. Ji MY, Vandenhole M, De Beer B, De Rouck S, Villacis-Perez E, Feyereisen R, Clark RM, Van Leeuwen T. A nuclear receptor HR96-related gene underlies large *trans*-driven differences in detoxification gene expression in a generalist herbivore. Nat Commun. 2023;14:4990.
63. Yang X, Deng S, Wei X, Yang J, Zhao Q, Yin C, Du TH, Guo ZJ, Xia JX, Yang ZZ, et al. MAPK-directed activation of the whitefly transcription factor CREB leads to P450-mediated imidacloprid resistance. Proc Natl Acad Sci. 2020;117:10246–53.
64. Hu C, Liu YX, Zhang SP, Wang YQ, Gao P, Li YT, Yang XQ. Transcription factor *AhR* regulates glutathione S-transferases conferring resistance to lambda-Cyhalothrin in *Cydia pomonella*. J Agric Food Chem. 2023;71:5230–9.
65. Gaddelapati SC, Kalsi M, Roy A, Palli SR. Cap'n'collar C regulates genes responsible for imidacloprid resistance in the Colorado potato beetle, *Leptinotarsa decemlineata*. Insect Biochem Mol Biol. 2018;99:54–62.
66. Zheng M, Tao W, Zou Y, Farokhzad OC, Shi B. Nanotechnology-based strategies for siRNA brain delivery for disease therapy. Trends Biotechnol. 2018;36:562–75.
67. Jain RG, Fletcher SJ, Manzie N, Robinson KE, Li P, Lu E, Brosnan CA, Xu ZP, Mitter N. Foliar application of clay-delivered RNA interference for whitefly control. Nature Plants. 2022;8:535–48.
68. Kolge H, Kadam K, Galande S, Lanjekar V, Ghormade V. New frontiers in pest control: chitosan nanoparticles-shielded dsRNA as an effective topical RNAi spray for gram podborer biocontrol. ACS Appl Bio Mater. 2021;4:5145–57.
69. Dhandapani RK, Gurusamy D, Palli SR. Development of catechin, poly-l-lysine, and double-stranded RNA nanoparticles. ACS Appl Bio Mater. 2021;4(5):4310–8.
70. Das S, Debnath N, Cui Y, Unrine J, Palli SR. Chitosan, carbon quantum dot, and silica nanoparticle mediated dsRNA delivery for gene silencing in *Aedes aegypti*: a comparative analysis. ACS Appl Mater Interfaces. 2015;7:19530–5.

71. Wang Z, Li M, Kong Z, Wang E, Zhang B, Lv J, Xu X. Star polycation mediated dsRNA improves the efficiency of RNA interference in *Phytoseiulus persimilis*. Nanomaterials. 2022;12:3809.
72. Chen A, Halilovic L, Shay JH, Koch A, Mitter N, Jin H. Improving RNA-based crop protection through nanotechnology and insights from cross-kingdom RNA trafficking. Curr Opin Plant Biol. 2023;76: 102441.

Publisher's Note